Supplementary figures and tables

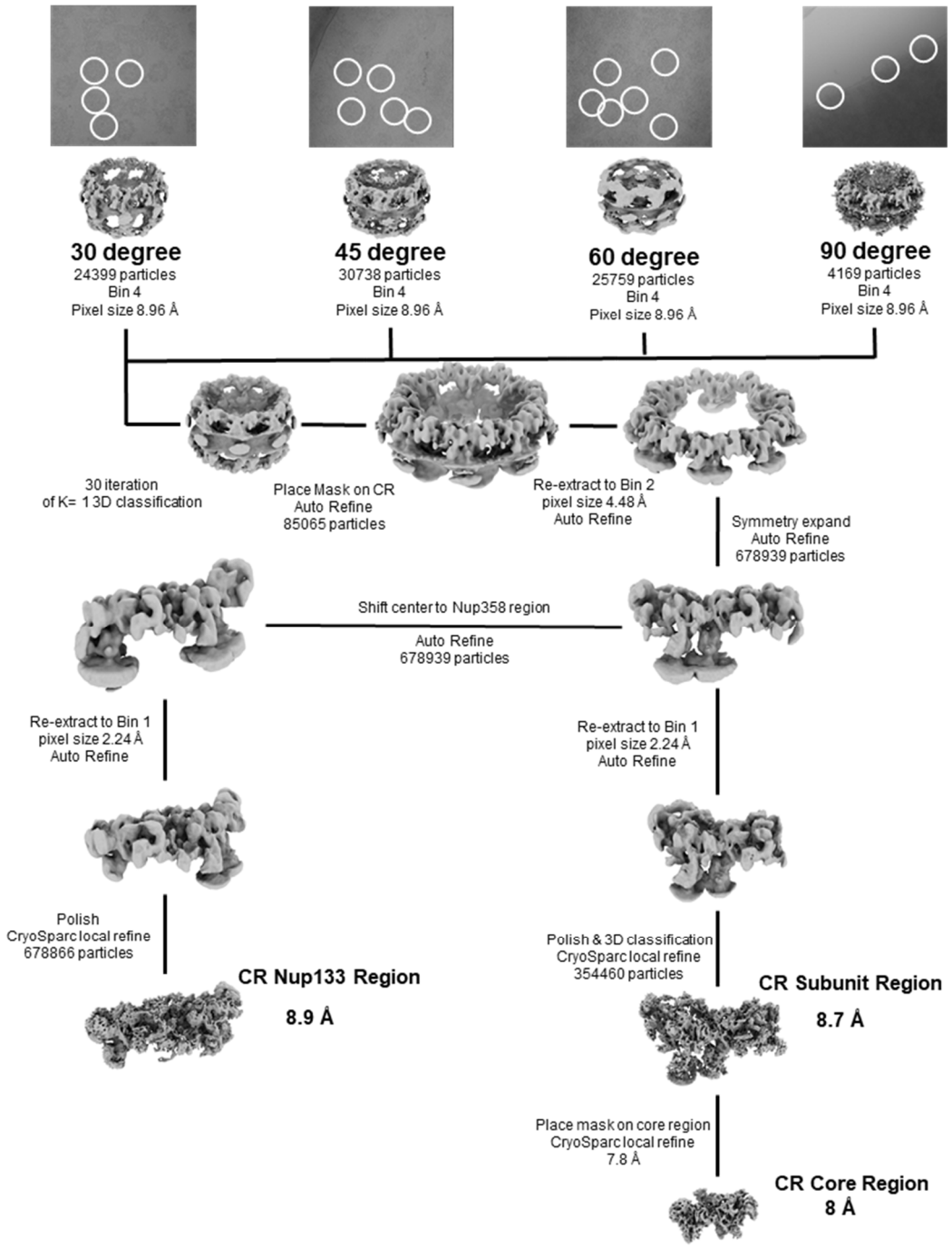

Figure S1. Data processing workflow of the CR from the *X. laevis* oocyte NPC.

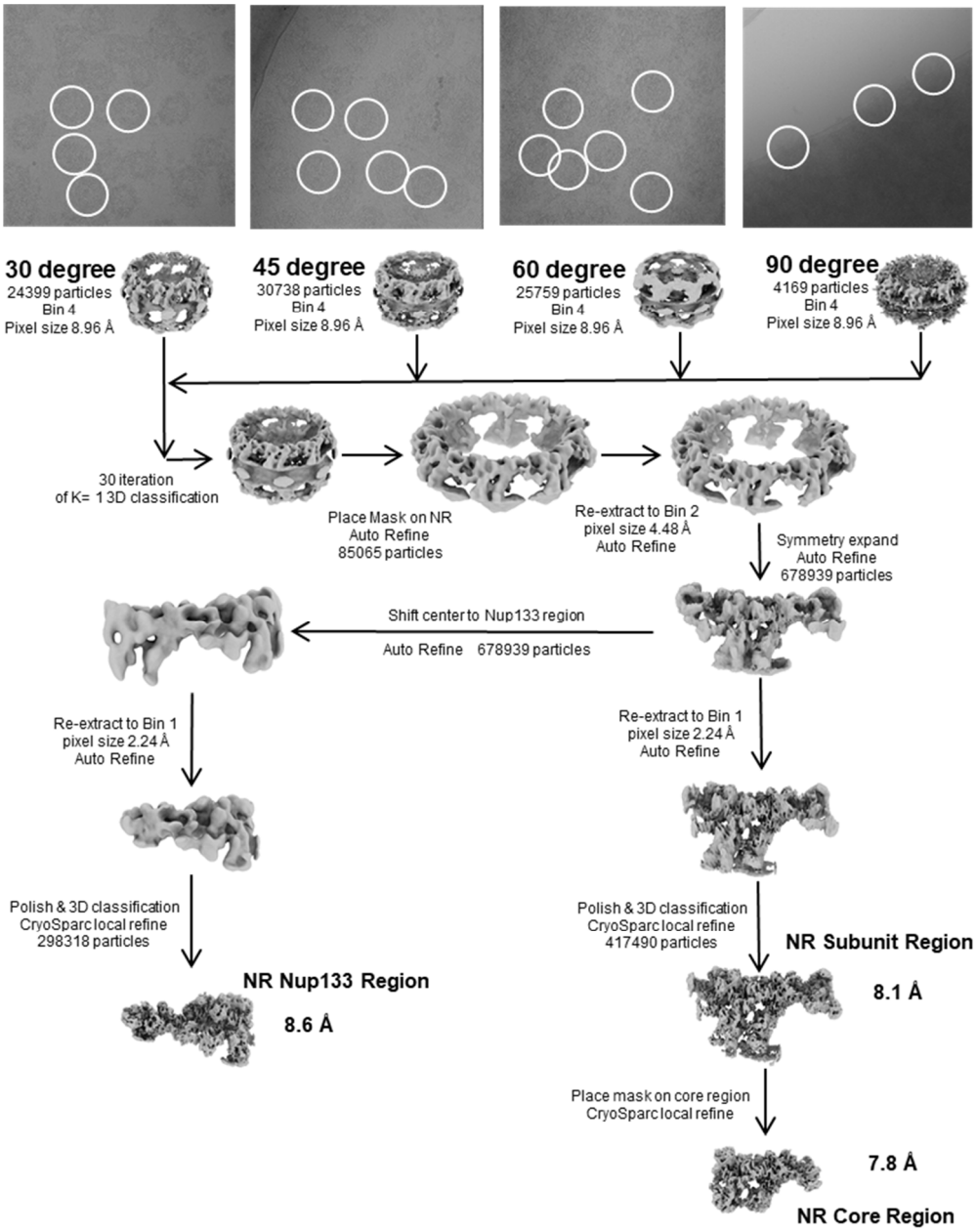

Figure S2. Data processing workflow of the NR from the *X. laevis* oocyte NPC.

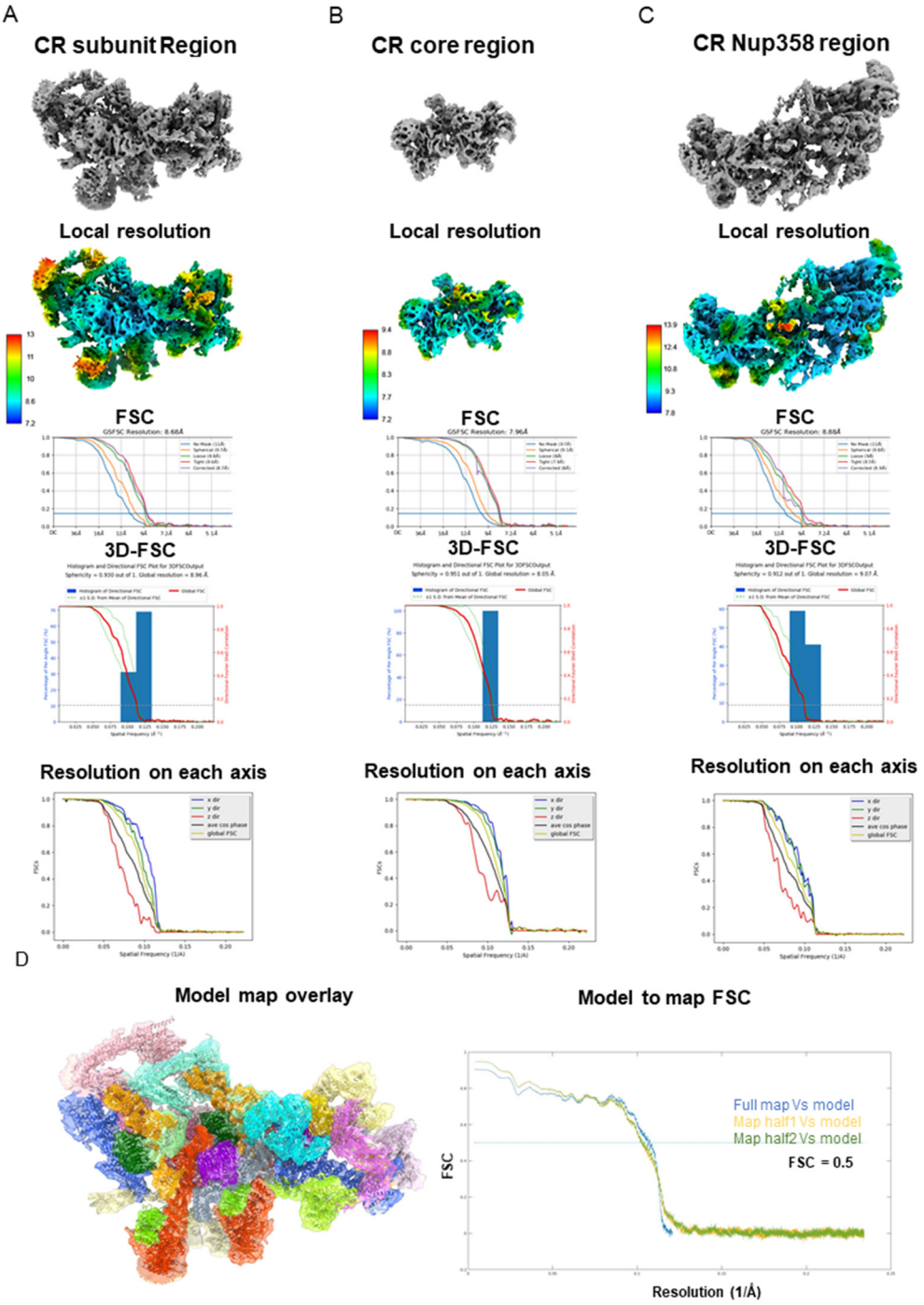

Figure S3. Assessments of cryo-EM maps of the CR subunit. (**A, B, C**) Map display, local resolution estimation, FSC, 3D-FSC and directional FSC of the CR subunit region, CR core region and CR Nup358 region. (**D**) Map model overlay of the CR subunit, and map versus model FSC estimation.

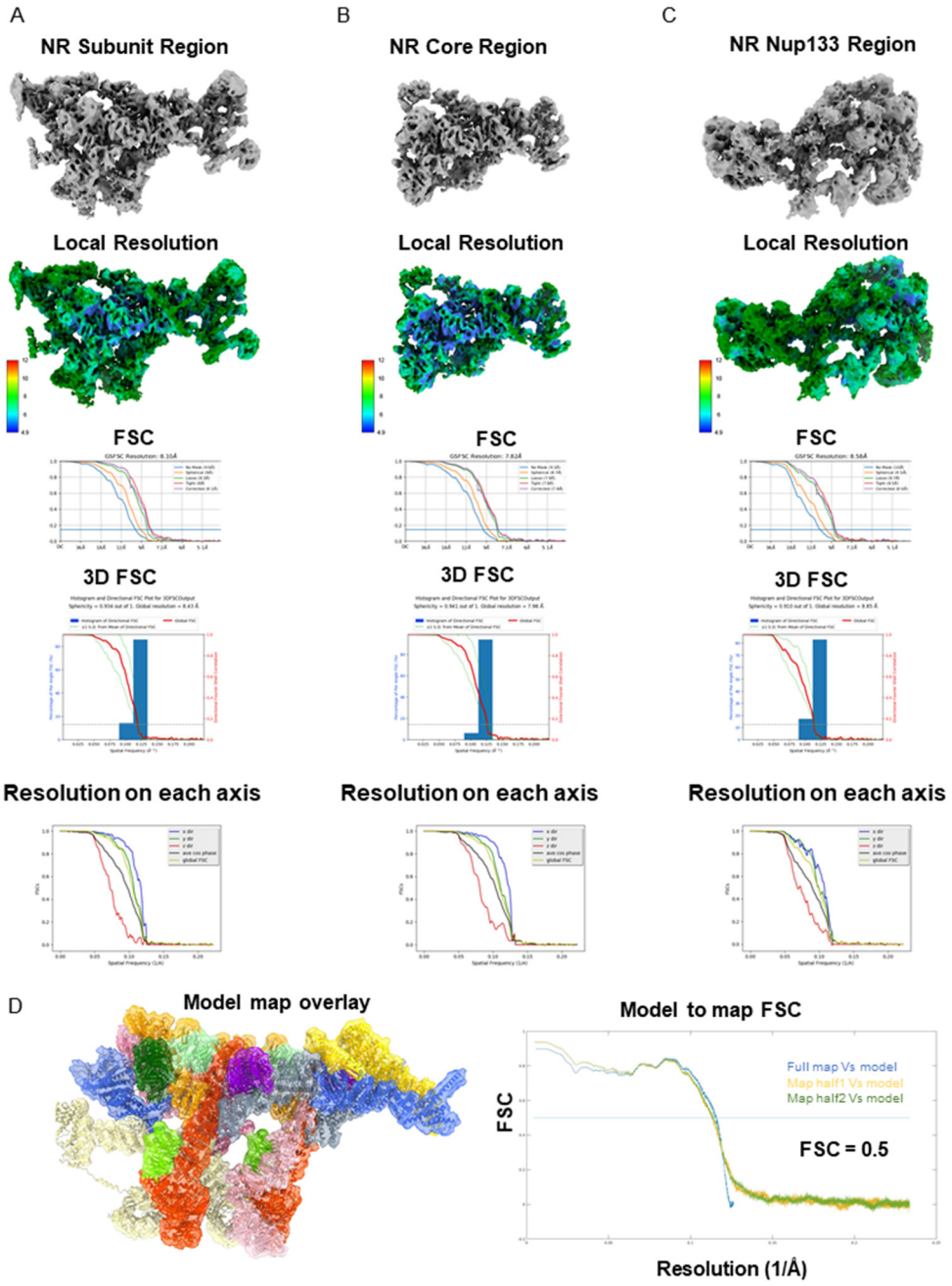

Figure S4. Assessments of cryo-EM maps of the NR subunit. (**A, B, C**) Map display, local resolution estimation, FSC, 3D-FSC and directional FSC of the NR subunit region, NR core region and NR Nup133 region. (**D**) Map model overlay of the NR asymmetric unit, and map versus model FSC estimation.

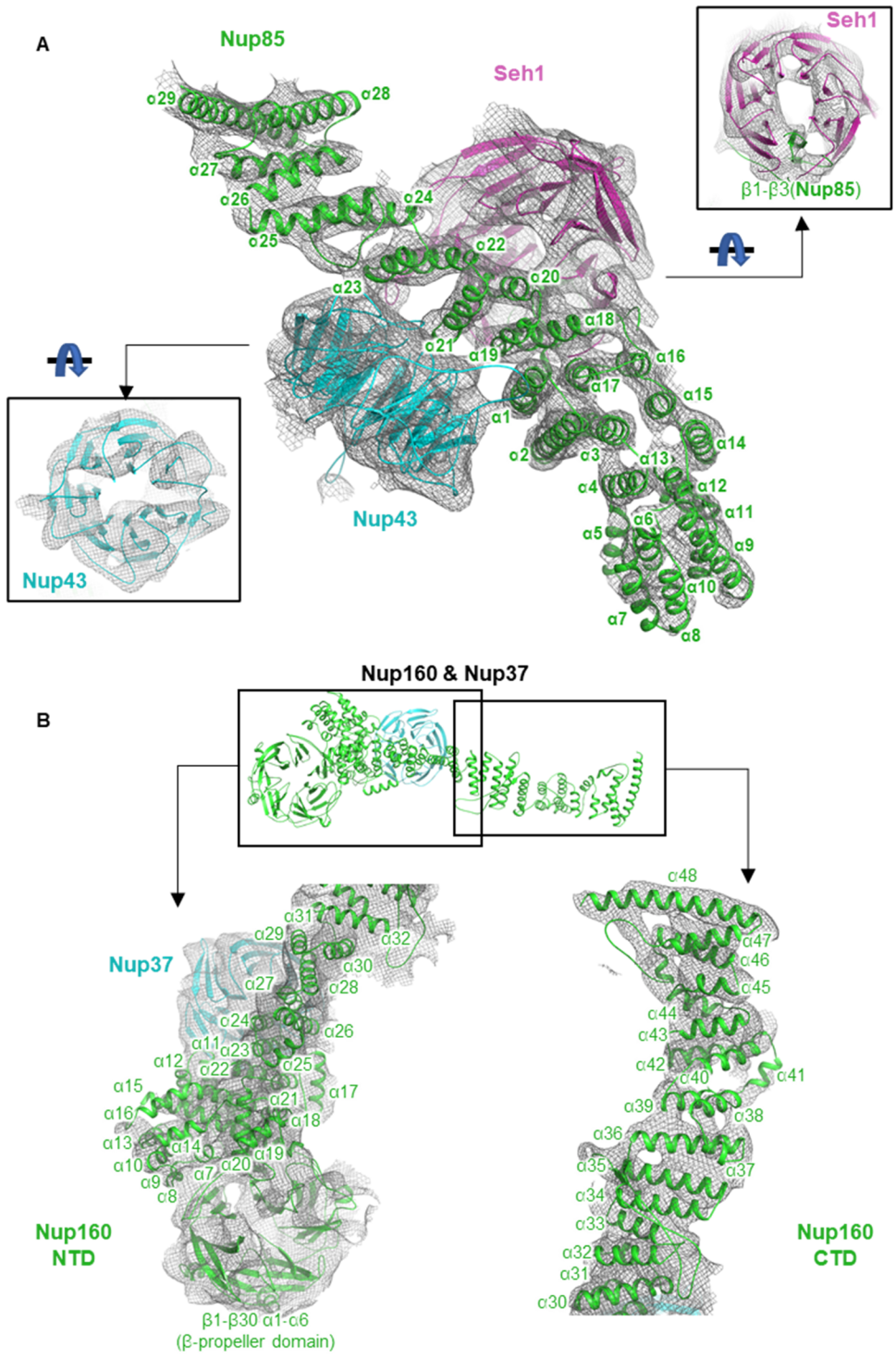
A
Nup85
Seh1
α29
α28
α27
α26
α25
α24
α22
α23
α20
α18
α21
α19
α16
α17
α15
α1
α14
α2
α3
α13
α4
α12
α11
α6
α5
α9
α10
α7
α8
Nup43
Nup43
Seh1
β1-β3(Nup85)
B
Nup160 & Nup37
Nup37
α31
α29
α32
α30
α27
α28
α24
α26
α11
α23
α12
α22
α25
α15
α17
α21
α16
α18
α13
α14
α19
α10
α7
α20
α9
α8
Nup160
NTD
β1-β30 α1-α6
(β-propeller domain)
α48
α47
α46
α45
α44
α43
α42
α41
α40
α39
α38
α36
α35
α37
α34
α33
α32
α31
α30
Nup160
CTD

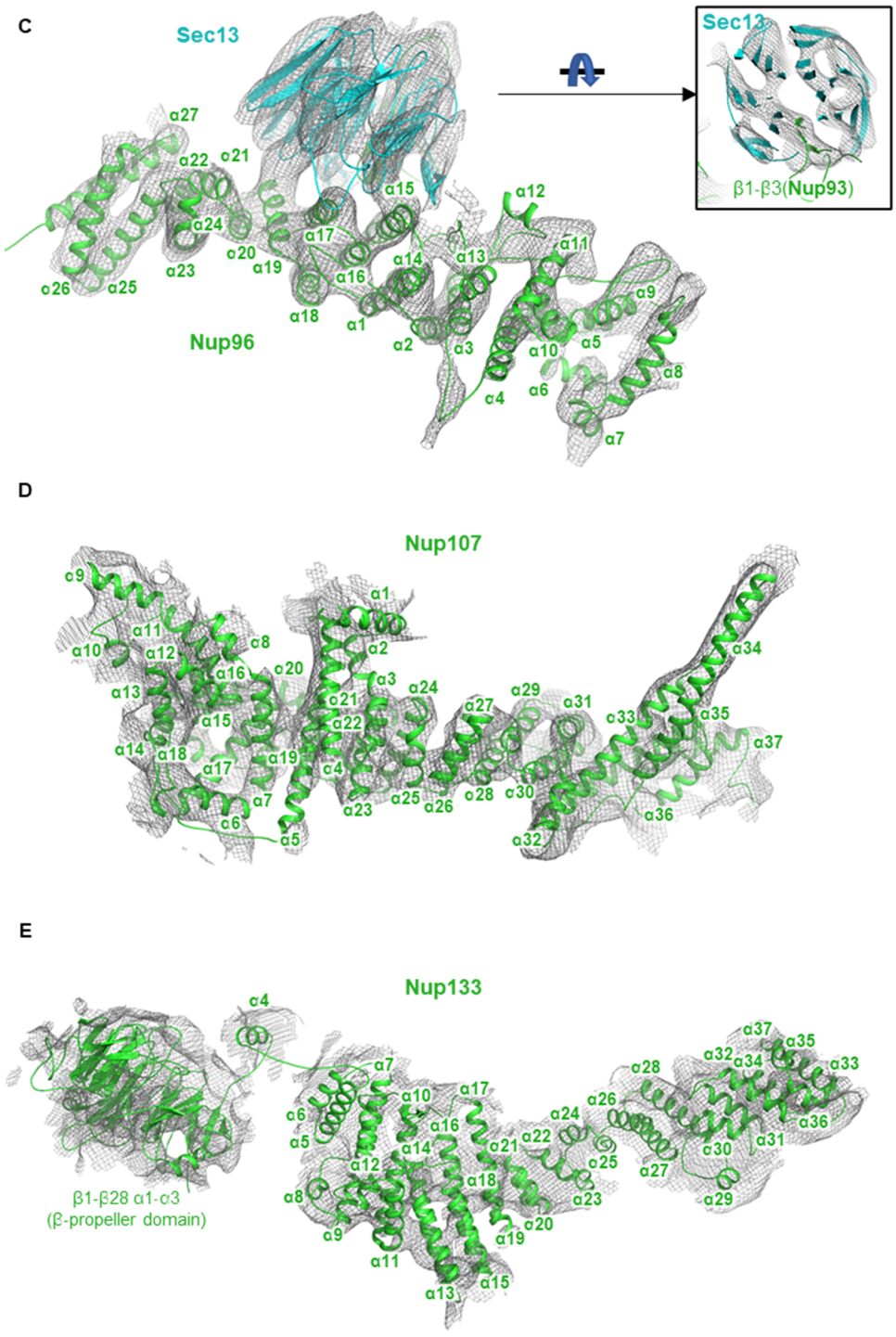
C
Sec13
α27
α22
α21
α24
α20
α19
α23
α26
α25
α17
α15
α16
α18
α1
α14
α13
α12
α11
α9
α2
α3
α10
α5
α8
α4
α6
α7
Nup96
Sec13
β1-β3(Nup93)
D
Nup107
α9
α11
α10
α12
α8
α16
α20
α13
α15
α14
α18
α17
α19
α7
α6
α5
α1
α2
α3
α24
α21
α22
α4
α23
α25
α26
α27
α28
α30
α29
α31
α33
α34
α35
α37
α36
α32
E
Nup133
α4
α7
α10
α6
α5
α17
α16
α14
α12
α8
α18
α9
α11
α13
α15
α21
α22
α24
α25
α23
α20
α19
α26
α28
α27
α30
α29
α31
α37
α35
α32
α34
α33
α36
β1-β28 α1-α3
(β-propeller domain)

F

Inner Nup205

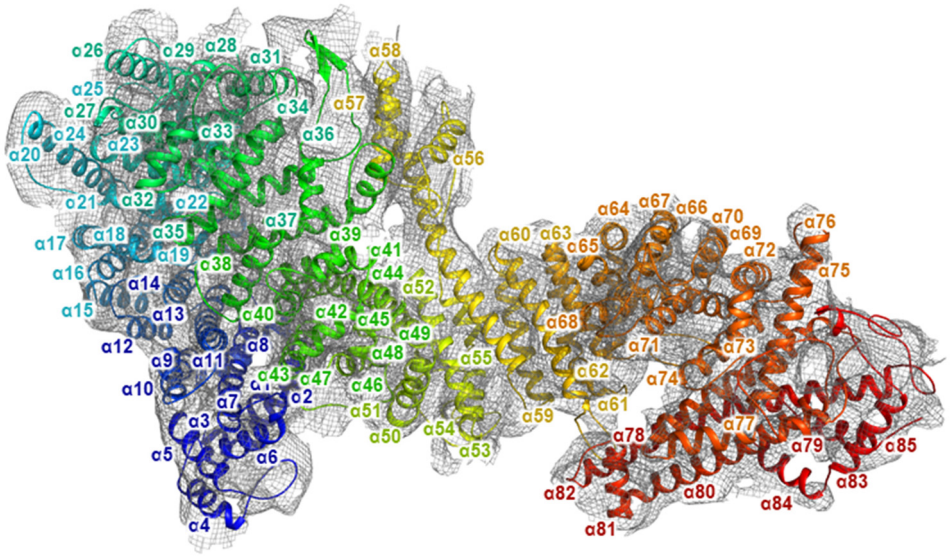

G

Outer Nup205

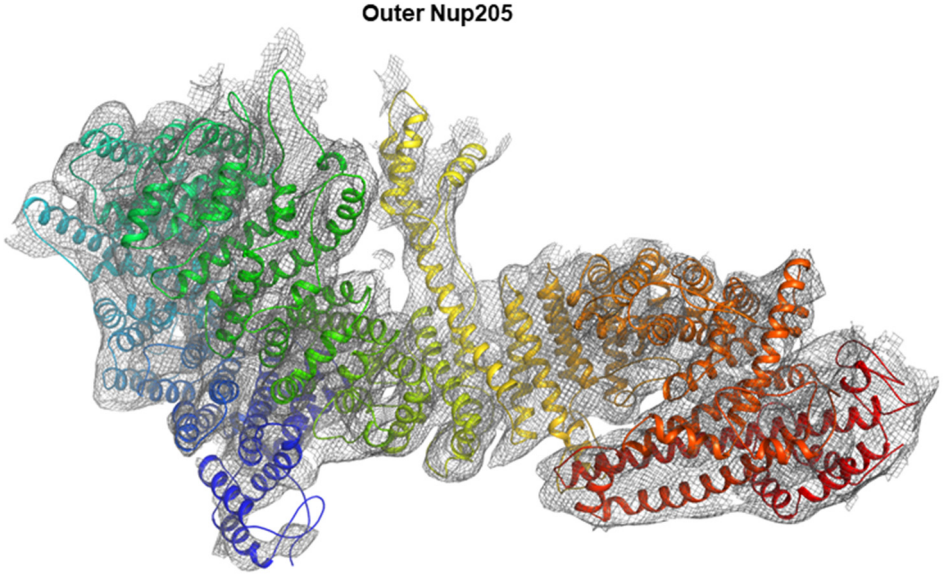

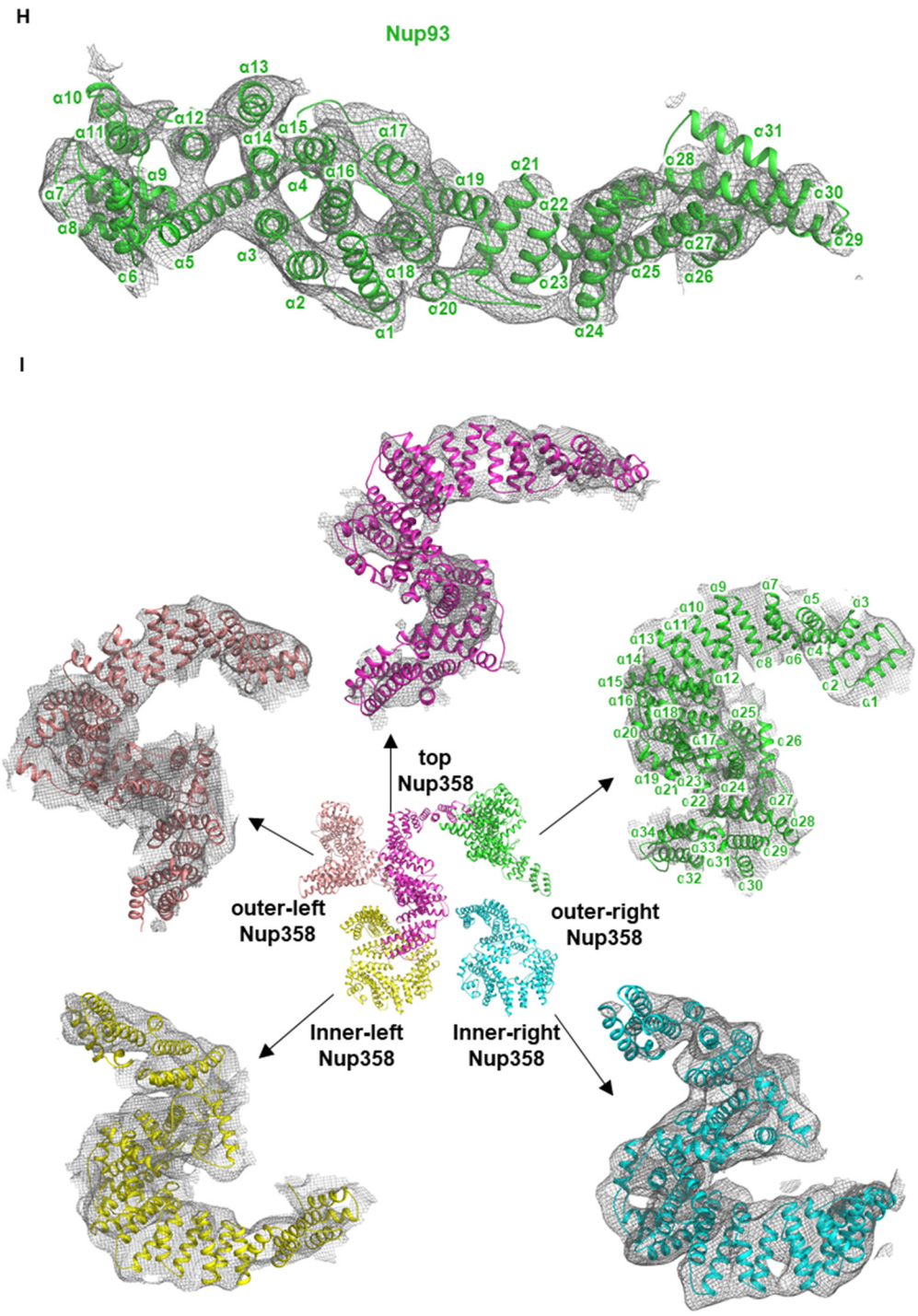
H
Nup93
α1
α2
α3
α4
α5
α6
α7
α8
α9
α10
α11
α12
α13
α14
α15
α16
α17
α18
α19
α20
α21
α22
α23
α24
α25
α26
α27
α28
α29
α30
α31
I
top
Nup358
outer-left
Nup358
outer-right
Nup358
Inner-left
Nup358
Inner-right
Nup358

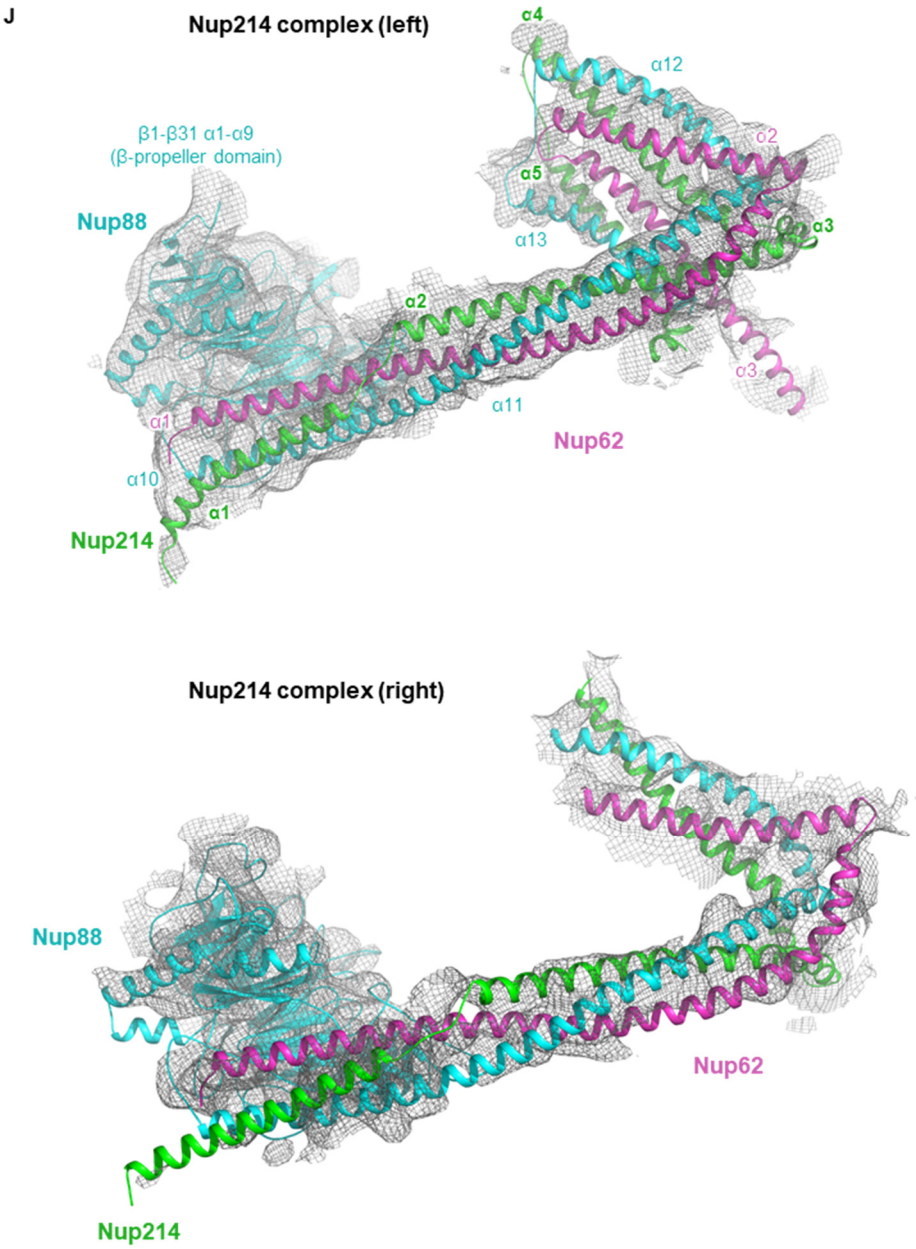

Figure S5. Model building quality and secondary structure assignment of the CR subunit. (A-J) Model building quality of Nup85, Seh1, Nup43, Nup160, Nup37, Sec13, Nup96, Nup107, Nup133, Nup205, Nup93, Nup358 and Nup214 complexes.

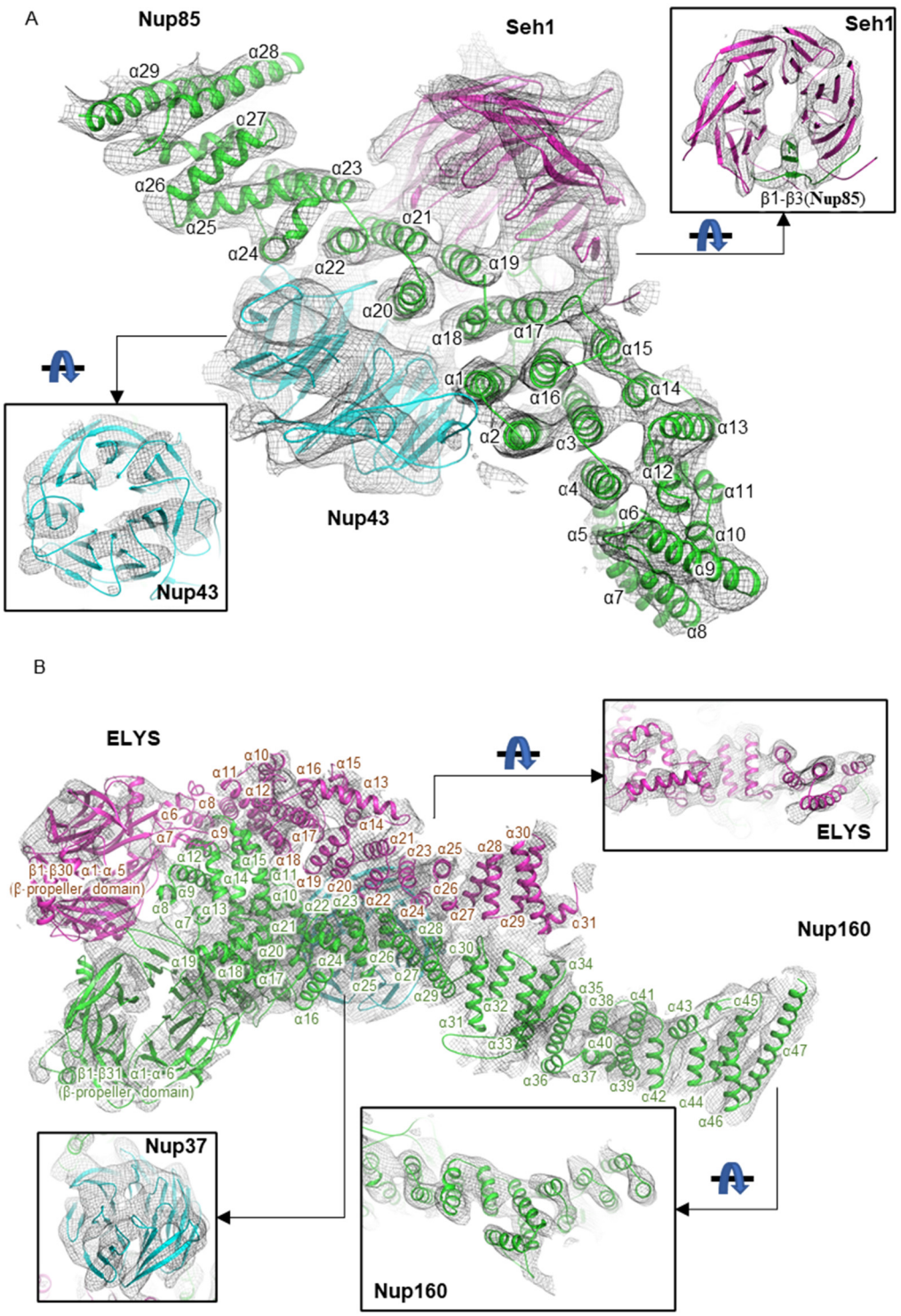
A
Nup85
Seh1
Seh1
β1-β3(Nup85)
Nup43
Nup43
α28
α29
α27
α26
α25
α24
α23
α22
α21
α20
α19
α18
α17
α16
α15
α14
α13
α12
α11
α10
α9
α8
α7
α6
α5
α4
α3
α2
α1
B
ELYS
ELYS
Nup160
Nup160
Nup37
β1-β30, α1-α5
(β-propeller, domain)
β1-β31, α1-α6
(β-propeller, domain)

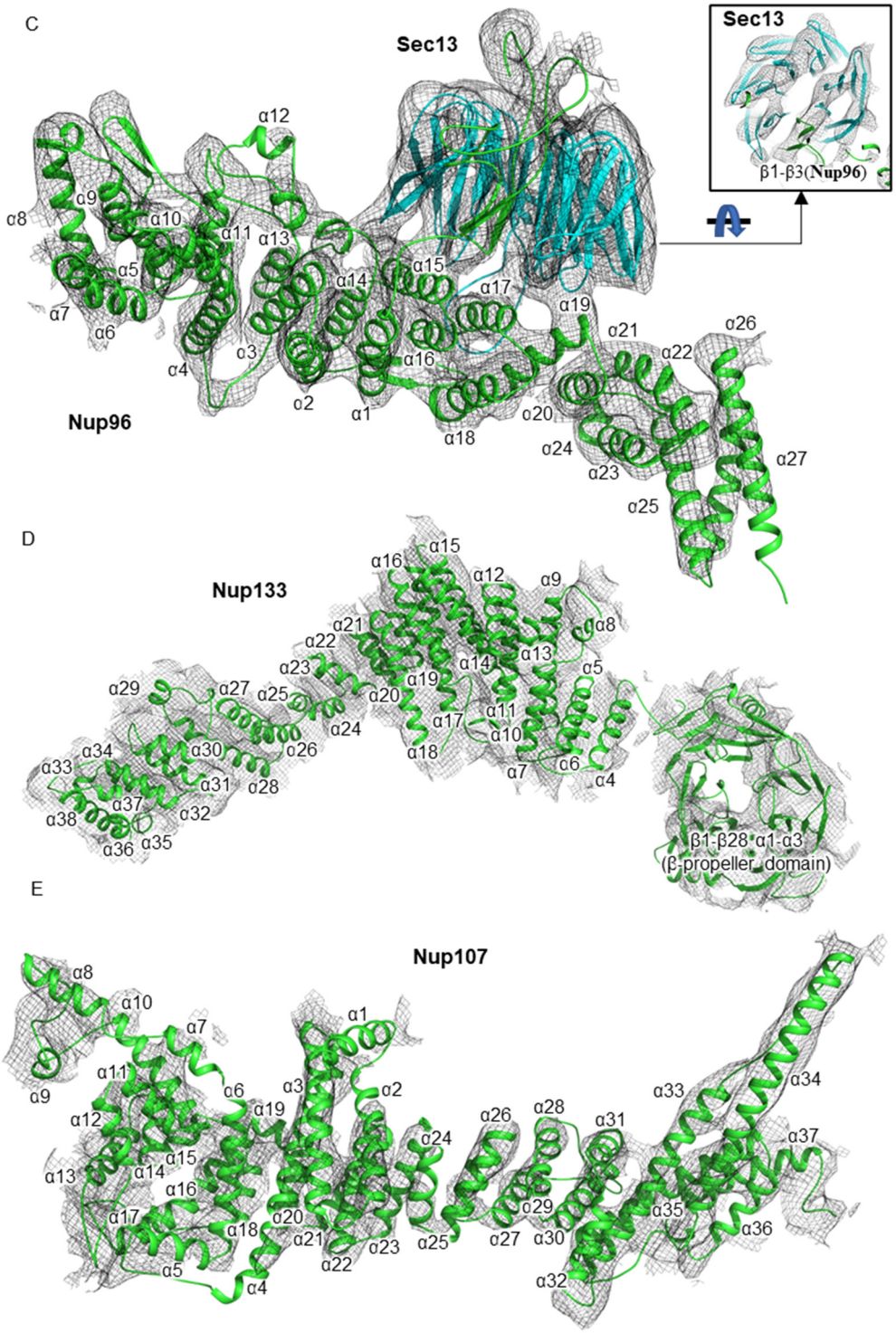
C
Sec13
Nup96
α1
α2
α3
α4
α5
α6
α7
α8
α9
α10
α11
α12
α13
α14
α15
α16
α17
α18
α19
α20
α21
α22
α23
α24
α25
α26
α27
Sec13
β1-β3(Nup96)
D
Nup133
α1
α2
α3
α4
α5
α6
α7
α8
α9
α10
α11
α12
α13
α14
α15
α16
α17
α18
α19
α20
α21
α22
α23
α24
α25
α26
α27
α28
α29
α30
α31
α32
α33
α34
α35
α36
α37
α38
β1-β28 α1-α3
(β-propeller_domain)
E
Nup107
α1
α2
α3
α4
α5
α6
α7
α8
α9
α10
α11
α12
α13
α14
α15
α16
α17
α18
α19
α20
α21
α22
α23
α24
α25
α26
α27
α28
α29
α30
α31
α32
α33
α34
α35
α36
α37

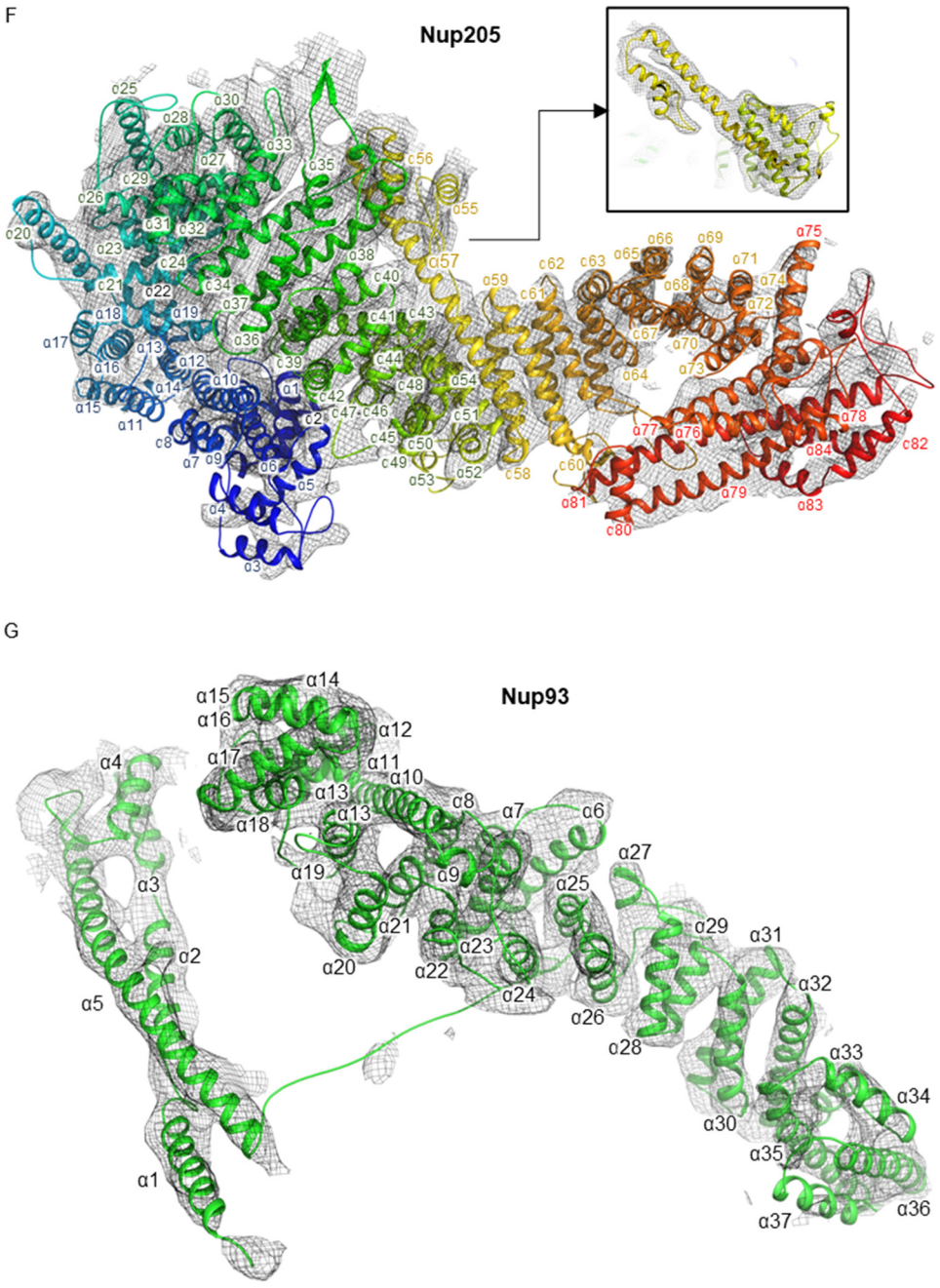

Figure S6. Model building quality and secondary structure assignment of the NR asymmetric unit. (A-G) Model building quality of Nup85, Seh1, Nup43, ELYS, Nup160, Sec13, Nup96, Nup133, Nup107, Nup205 and Nup93.

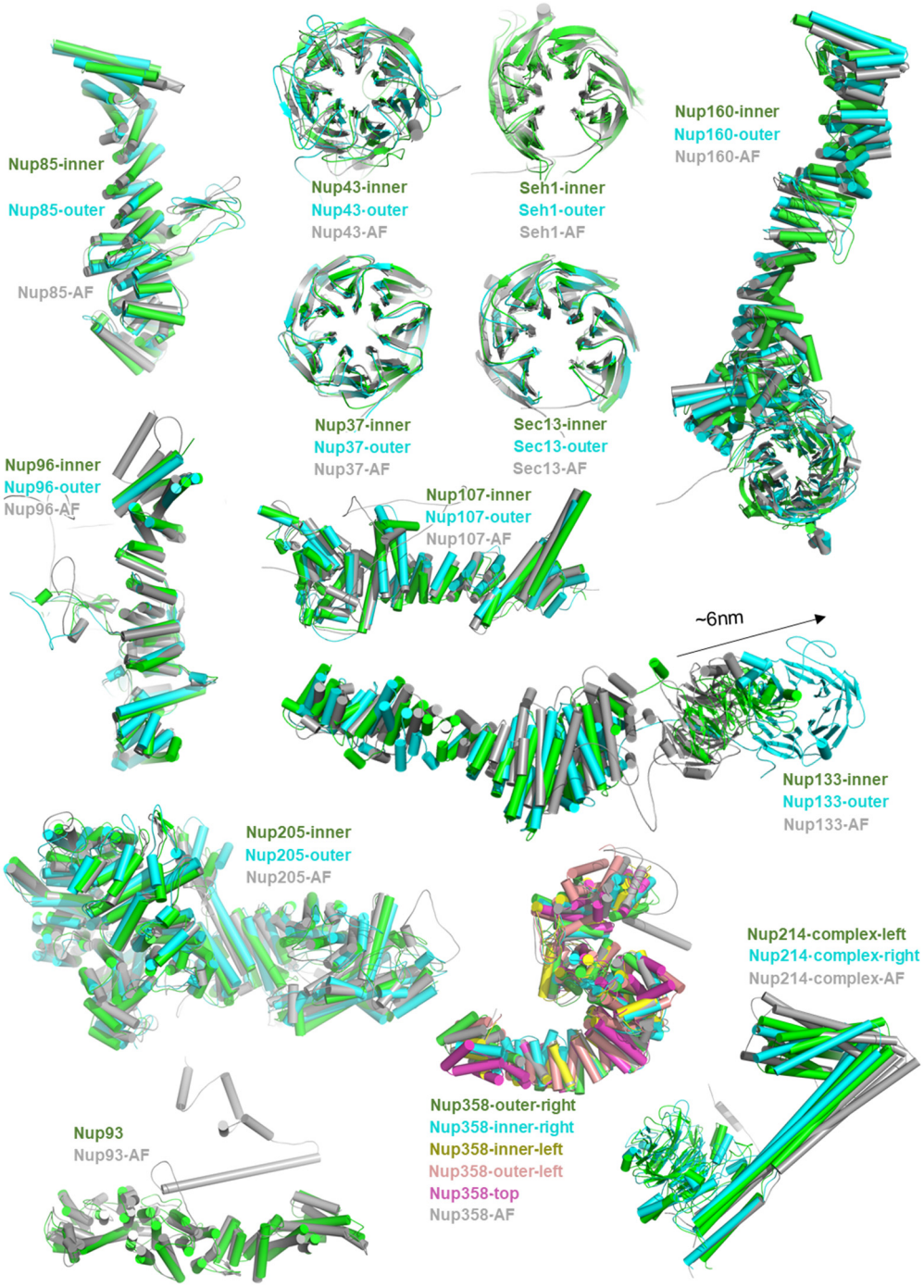

Figure S7. Comparisons of the refined structure and predicted structure by AlphaFold2 (AF) of CR Nups from the *X. laevis* NPC.

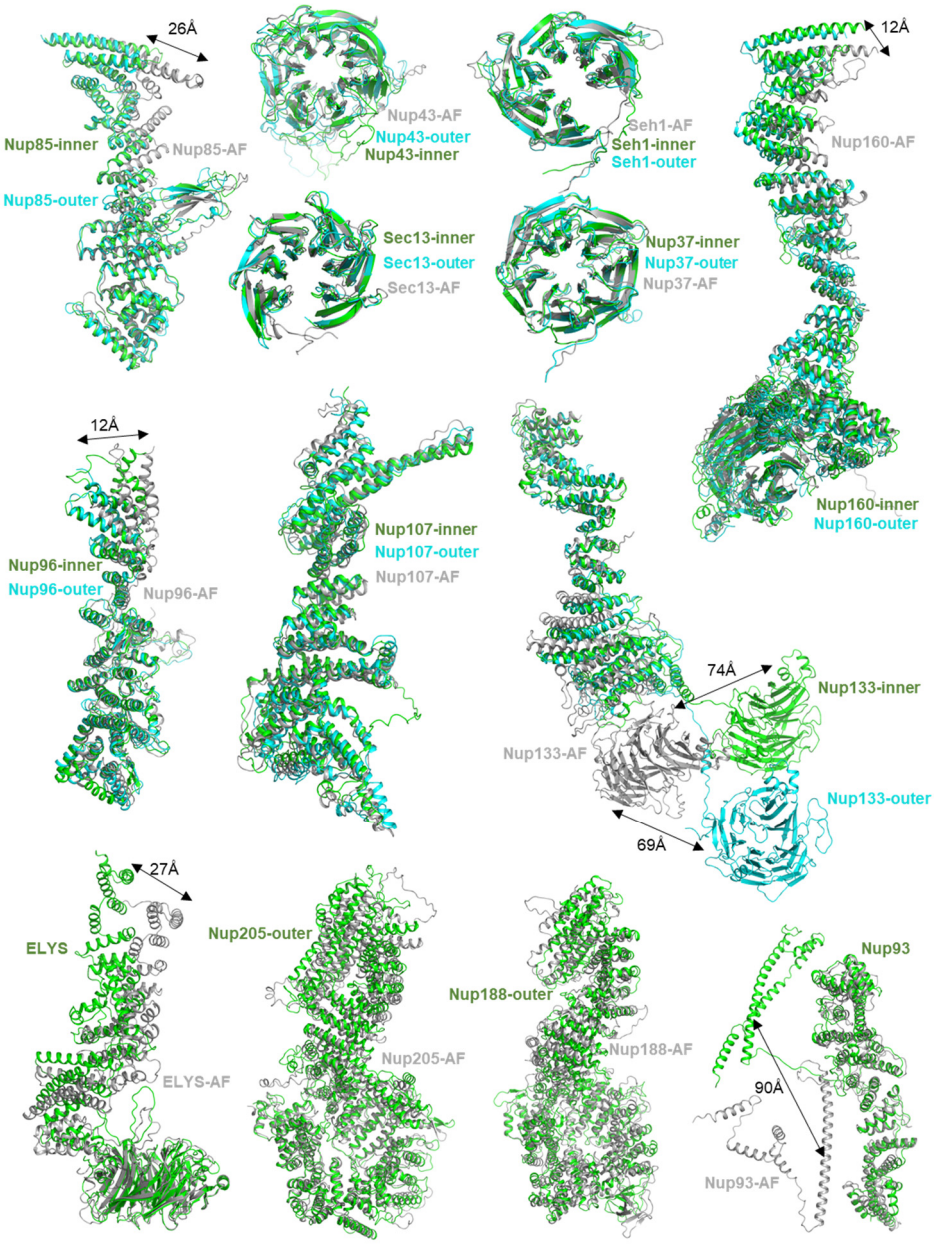

Figure S8. Comparisons of the refined structure and predicted structure by AlphaFold2 (AF) of NR Nups from the *X. laevis* NPC.

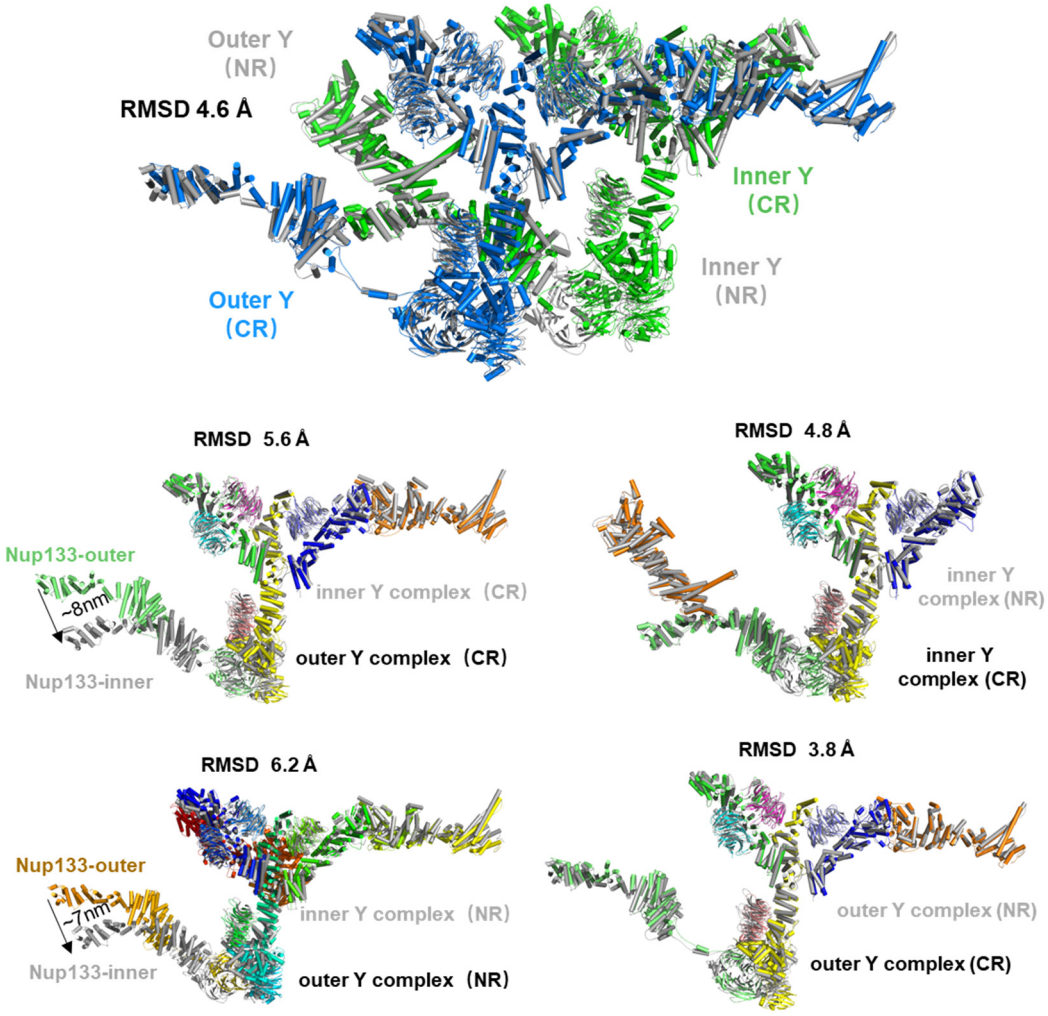

Figure S9. Structural comparations of Y-complexes in NR & CR from *X. laevis* NPC.

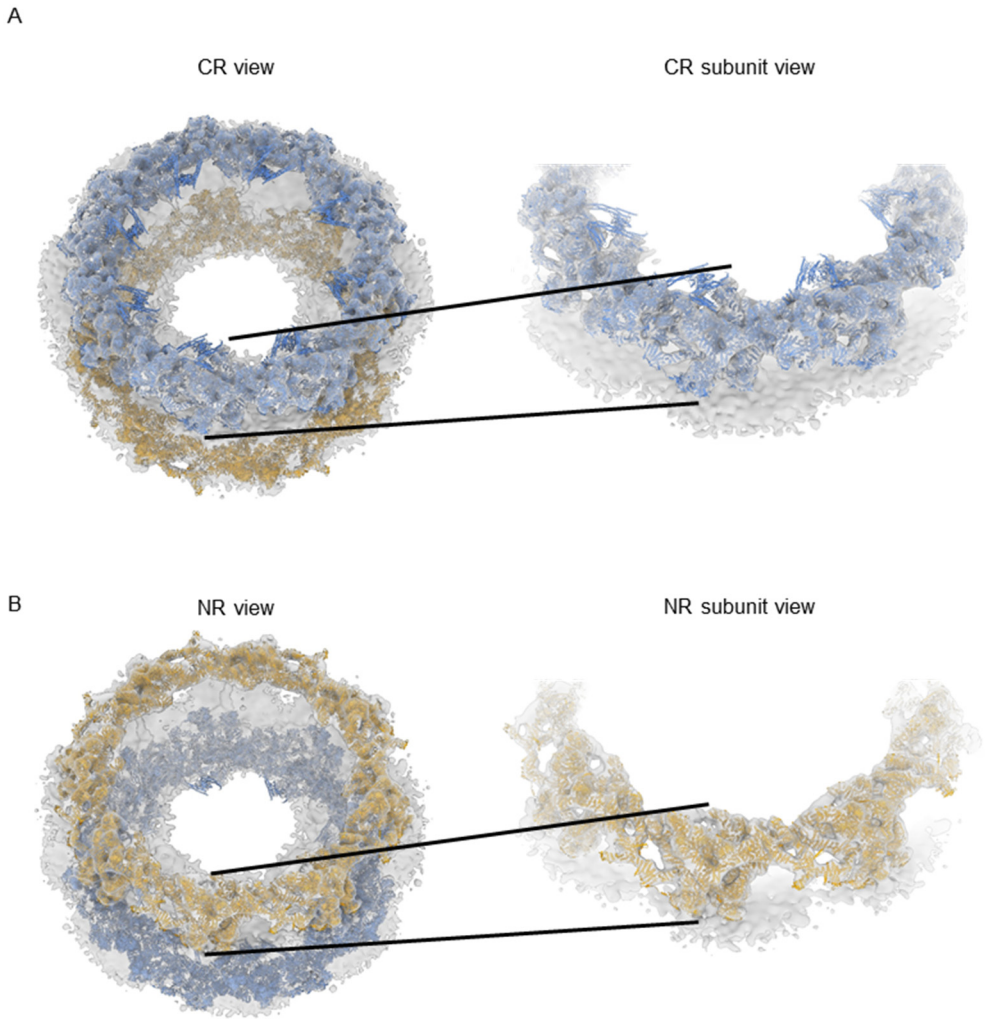

Figure S10. CR and NR models of *X. laevis* NPC fitted in human NPC map (EMD-3103).

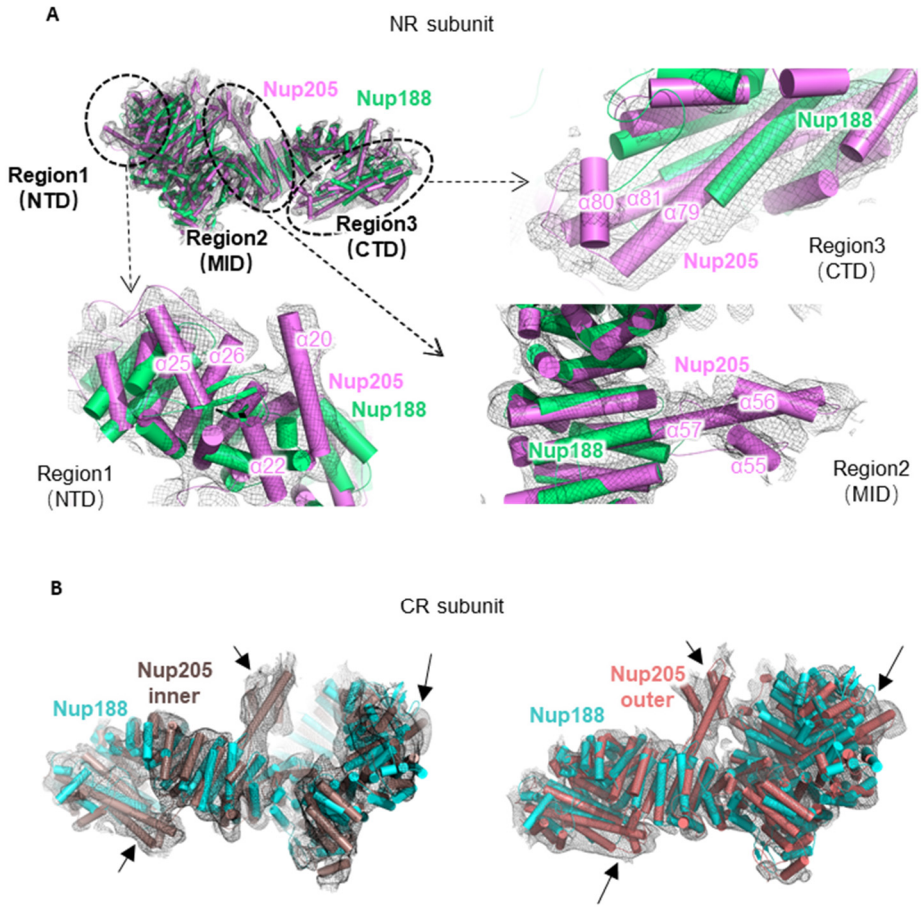

Figure S11. Nup205, instead of Nup188, is located in NR and CR. (A) Model comparison of Nup205 and Nup188 onto local densities in NR subunit. Major differences are enlarged and displayed in detail. (**B**) Model comparison of Nup205 and Nup188 onto local densities in CR subunit. The cryo-EM density maps are shown as a black mesh.

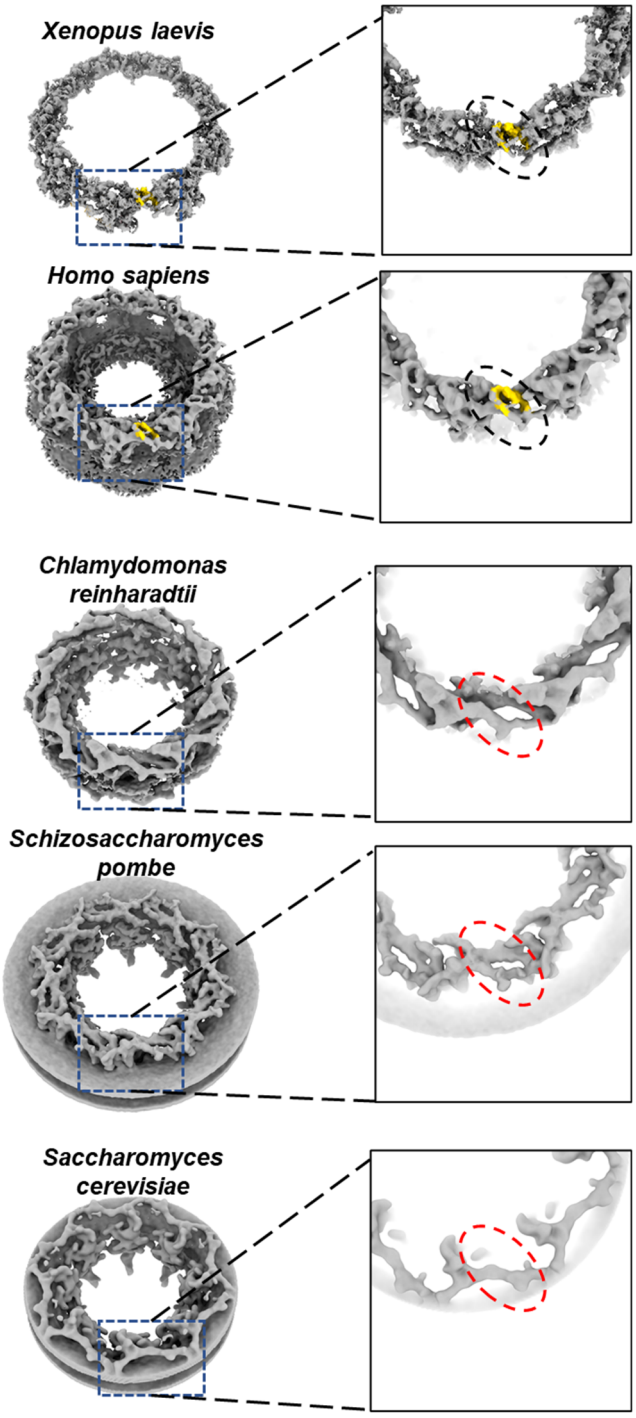

Figure S12. Comparisons of bridge-like densities in the NPC NR for different species.

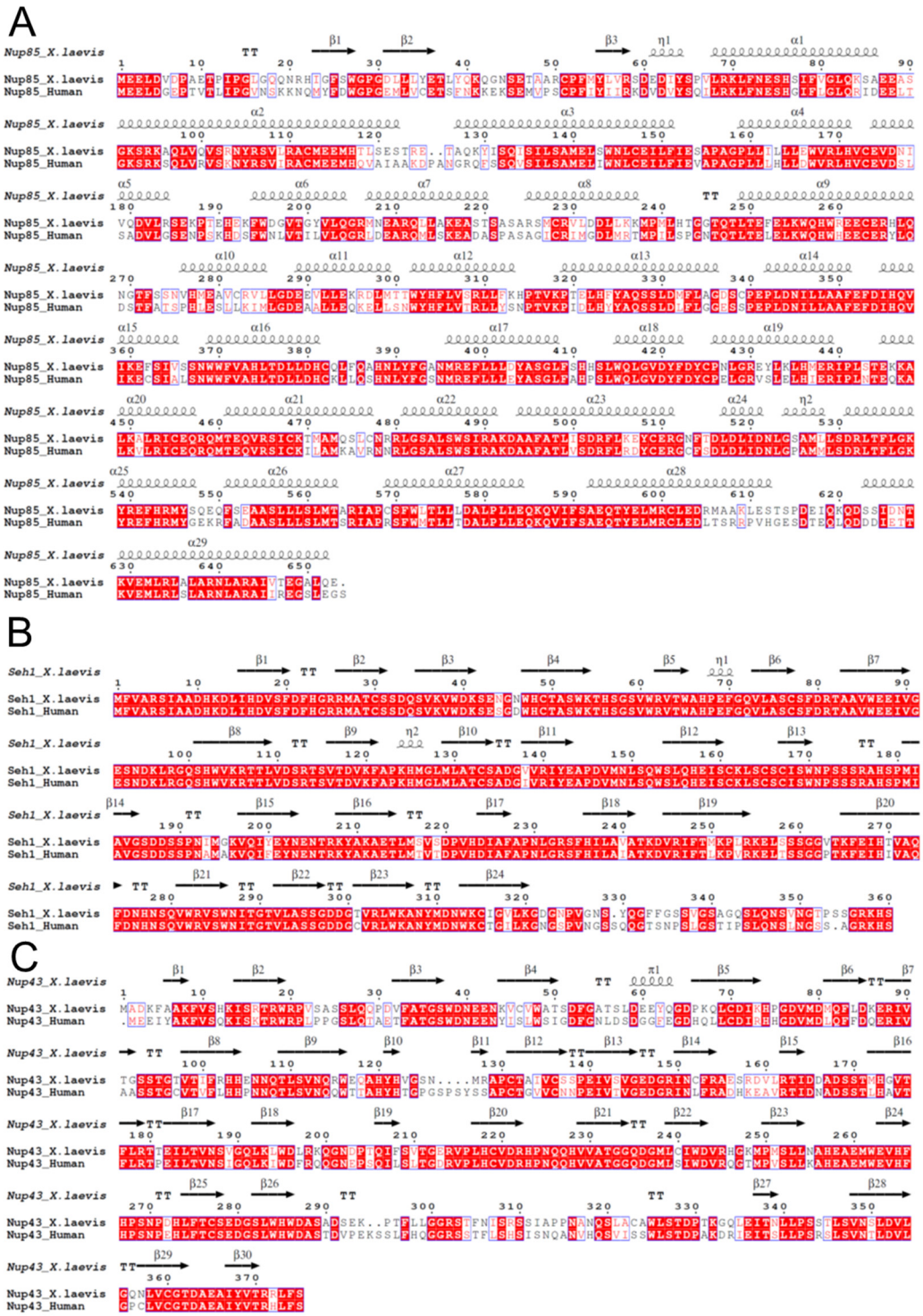
A
Nup85_X.laevis
Nup85_Human
B
Seh1_X.laevis
Seh1_Human
C
Nup43_X.laevis
Nup43_Human

D

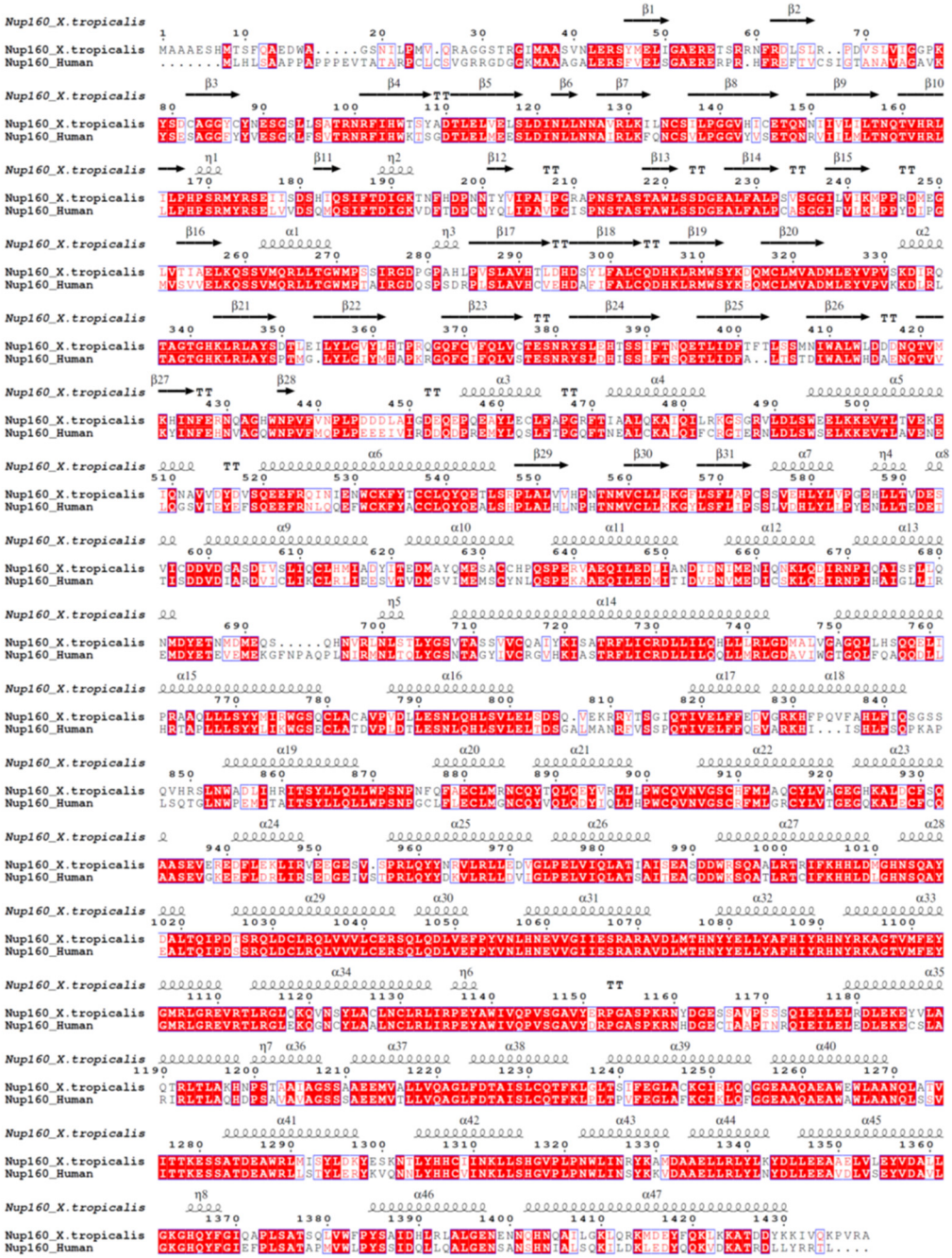

E

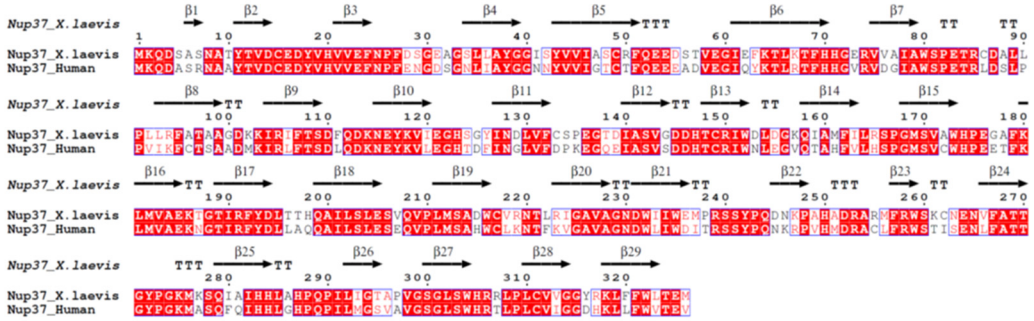

F

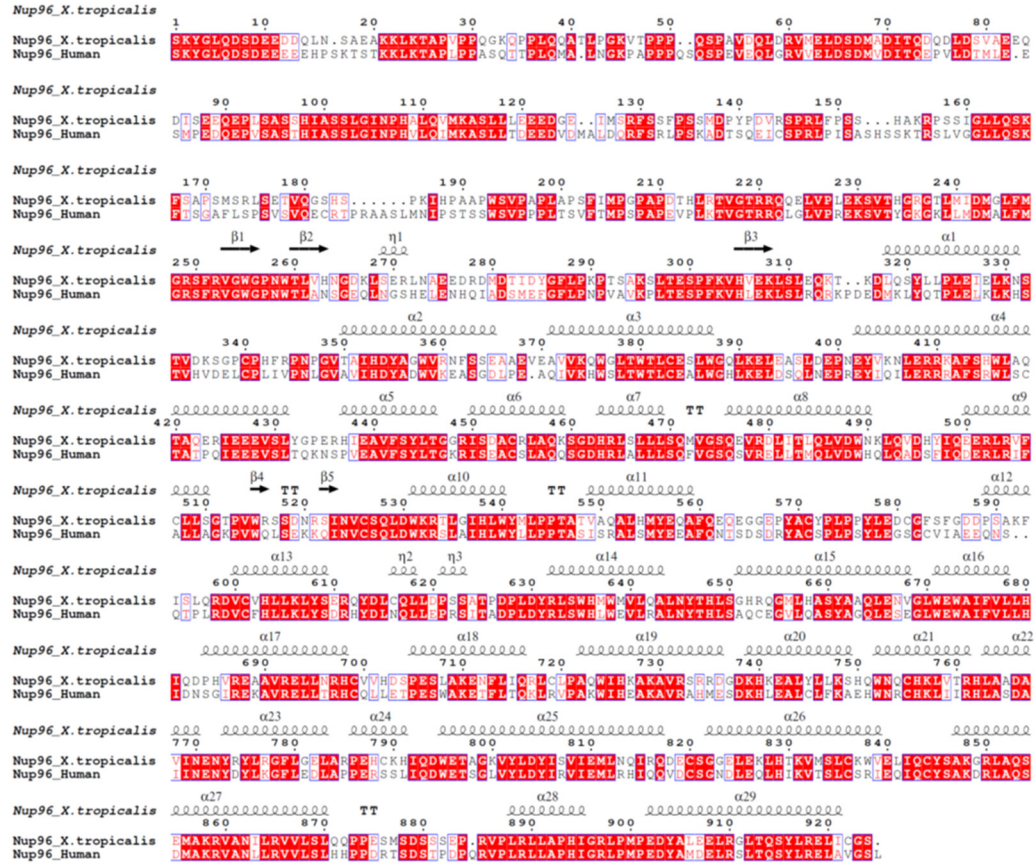

G

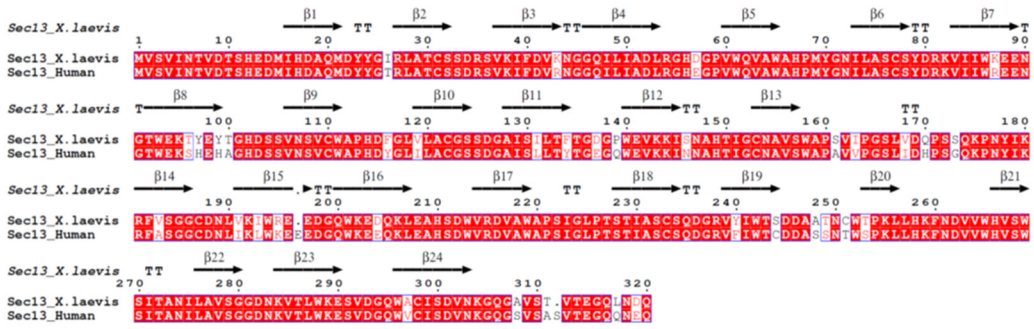
Sec13_X.laevis
Sec13_Human
MVSVINTVDTSHEDMIHDAQMDYYGRLATCSSDRSVKIFDVENGGQILIADLRGHEGPVWQVAWAHPMYGNILASCSYDRKVIIWKEEN
MVSVINTVDTSHEDMIHDAQMDYYGRLATCSSDRSVKIFDVENGGQILIADLRGHEGPVWQVAWAHPMYGNILASCSYDRKVIIWREEN
GTWEKTYEYTGHDSSVNSVCWAPHDEGLVLACGSSDGAISILTFTGEGPWEVKKISNAHTIGCNAVSWAPSVIPGSLVDQRSSQKPNYIK
GTWEKSHEHAGHDSSVNSVCWAPHDEGLILACGSSDGAISLLTFTGEGQWEVKKINNAHTIGCNAVSWAPAVVPGSLEDHPSGQKPNYIK
RFVSGGCDNLVKIWREEDGQWKEEQKLEAHSDWVRDVAWAPSIGLPTSTIASCSQDGRVFIWTSDDAFNCWEPKLLHKFNDVVWHVSW
RFASGGCDNLIKIWREEDGQWKEEQKLEAHSDWVRDVAWAPSIGLPTSTIASCSQDGRVFIWTCDDASNTWEPKLLHKFNDVVWHVSW
SITANILAVSGGDNKVTLWKESVDGQWECISDVNKGQGAVSTVTEGQLNDQ
SITANILAVSGGDNKVTLWKESVDGQWVCISDVNKGQGSVSASVTEGQQNEQ

H

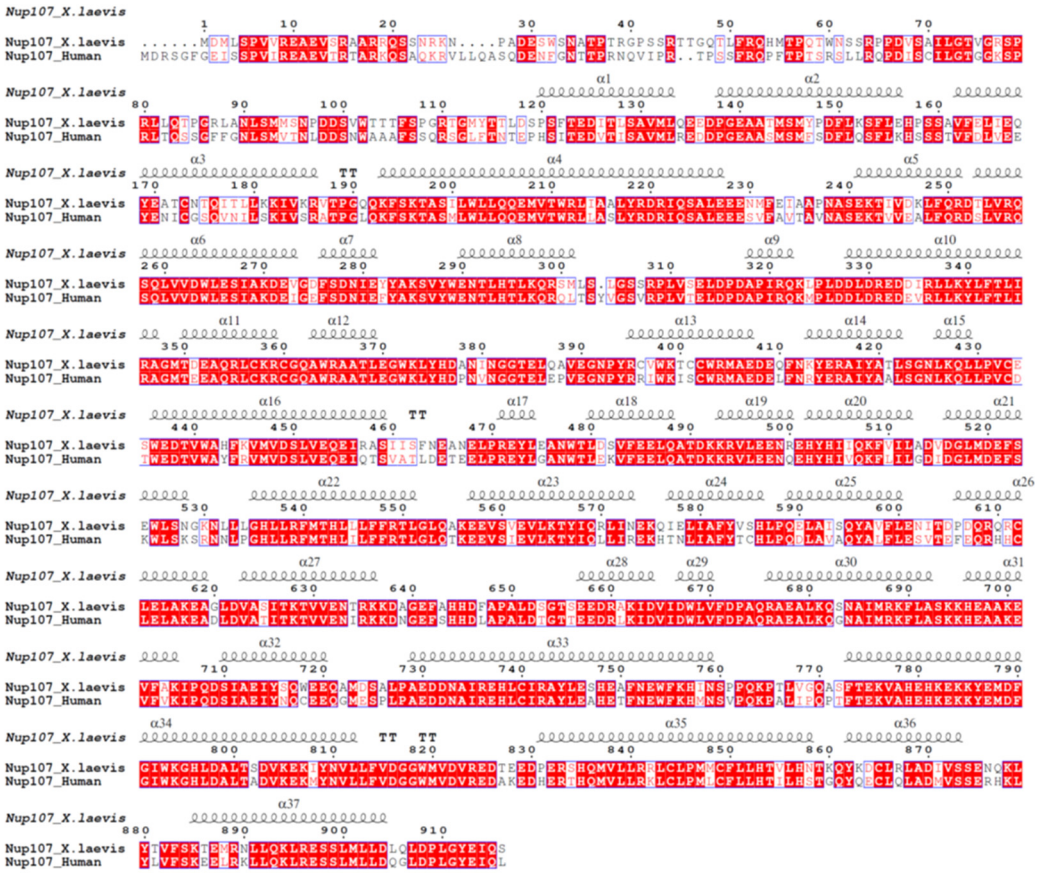
Nup107_X.laevis
Nup107_Human
.....MDMLSPVTREAEVFRAARRQSSNRKN....PADESWSNATPTRGPSSRTTGQTLFRQHMTPQTWNSSRPPDRSAILGTVGRSP
MDRSGFGEISSPVTREAEVHRTARMQSAQKRVLLQASQDENFGNTTPRNQVIPR..TPSSFRQPFTPTSRSLLRQPDHSCILGTGGKSP
RLLQTPGRLANLSMSNPDDSVWTTTFSPGRTGMYTTLDSPSFTEDLTFSAVMLQEPDPGEAATMSMVPDFLKSFLEHSSAVFSLHEQ
RLTQSSGFFGNLSMVTNIDDSNWAAAFSSQRSGLFTNTEPHSITEDVTFSAVMLREPDPGEAASMSMESDFLQSFLKHSSHVFSLMEE
YEATCNTQITLLKKIVKRVTPGQQKFSKTASILWLLQQEMVTWRLHAALYRDRIQSALEEENMFEIAPNASEKTHVDKLFQRDTLVRQ
YENICGSQVNILSKIVSRATPGLQKFSKTASMLWLLQQEMVTWRLHASLYRDRIQSALEEESVFAVTAVNASEKTWVEALFQRDSLVRQ
SQLVVDWLESIAKDEVGFSDNIEYYAKSVYWENTLHTLKQRSMLS.FGSSRPLVSELDPDAPIRQKFPLDDLDREDIRLLKYLFTLI
SQLVVDWLESIAKDEHGFSDNIESYAKSVYWENTLHTLKQRQLTSYVGSSRPLVTELDPDAPIRQKSPLDDLDREDVRLLKYLFTLI
RAGMTPEAQRLCKRCGQAWRAATLEGWKLYHDANINGGTELQAVEGNPYRCVWKTCCWRMAEDEQFNSYERAIYAHLSGNLKQLLPVCE
RAGMTSEAQRLCKRCGQAWRAATLEGWKLYHDPNVNGGTELEPVEGNPYRRIWKISCWRMAEDEHFNSYERAIYAALSGNLKQLLPVCD
SWEDTVWAHFKVMVDSLVEQEIRASIISFNSANELPREYLEANWTLDSVFEELQATDKKRVLEENREHYHIHQKFVILADVDGLMDEFS
TWEDTVWAVFRVMVDSLVEQEIQTSVATLLDETELPREYLGANWTLEKVFEELQATDKKRVLEENQEHYHINQKFHILGDHDGLMDEFS
EWLSNGRNLLLGHLLRFMTHLLFFRTLGLQAKEEVSVEVLKTYIQRLINEKQIELIAFYVSHLPQELAISQYAVFLENITDPDQRQRC
KWLSKSRNNLPGHLLRFMTHLHLFFRTLGLQTKEEVSHEVLKTYIQLLIREKHTNLIAFYTCHLPQDLAVAQYAFFLESVTEFEQRHRC
LELAKEAGLDVASITKTVVENTRKKDAGEFAHHDFAPALDSGTSEEDRAKIDVIDWLVFDPAQRAEALKQSNAIMRKFLASKKHEAAKE
LELAKEADLDVAHITKTVVENTRKKDRGEFSHHDFAPALDHGTHEEDRLKIDVIDWLVFDPAQRAEALKQCNAIMRKFLASKKHEAAKE
VFAKIPQDSIAEIYSQNEEQAMPSALPAEDDNAIREHLCIRAYLESHEAFNEWFKHINSPPQKPTLVSQASFTEKVAHEHKEKKYEMDF
VFSKIPQDSIAEIYNQSEEQGMPSPLPAEDDNAIREHLCIRAYLEAHETFNEWFKHMNSVPQKPALIPQPHFTEKVAHEHKEKKYEMDF
GIWKGHLDALTSDVKEKMYNVLLFVDGGWMVDVREDTEEDRERSHQMVLLRSLCLPMSCFLLHTSLHSTKQYKPCLRLADMVSSENQKL
GIWKGHLDALTADVKEKMYNVLLFVDGGWMVDVREDAKEDRERGHQMVLLRSLCLPMSCFLLHTSLHSTGQYQPCLQLADMVSSERHKL
YTVFSKTEVRNLLQKLRESSLMLLDLGLDPLGYEIQS
YLVFSKEELRKLLQKLRESSLMLLDQGLDPLGYEIQL

I

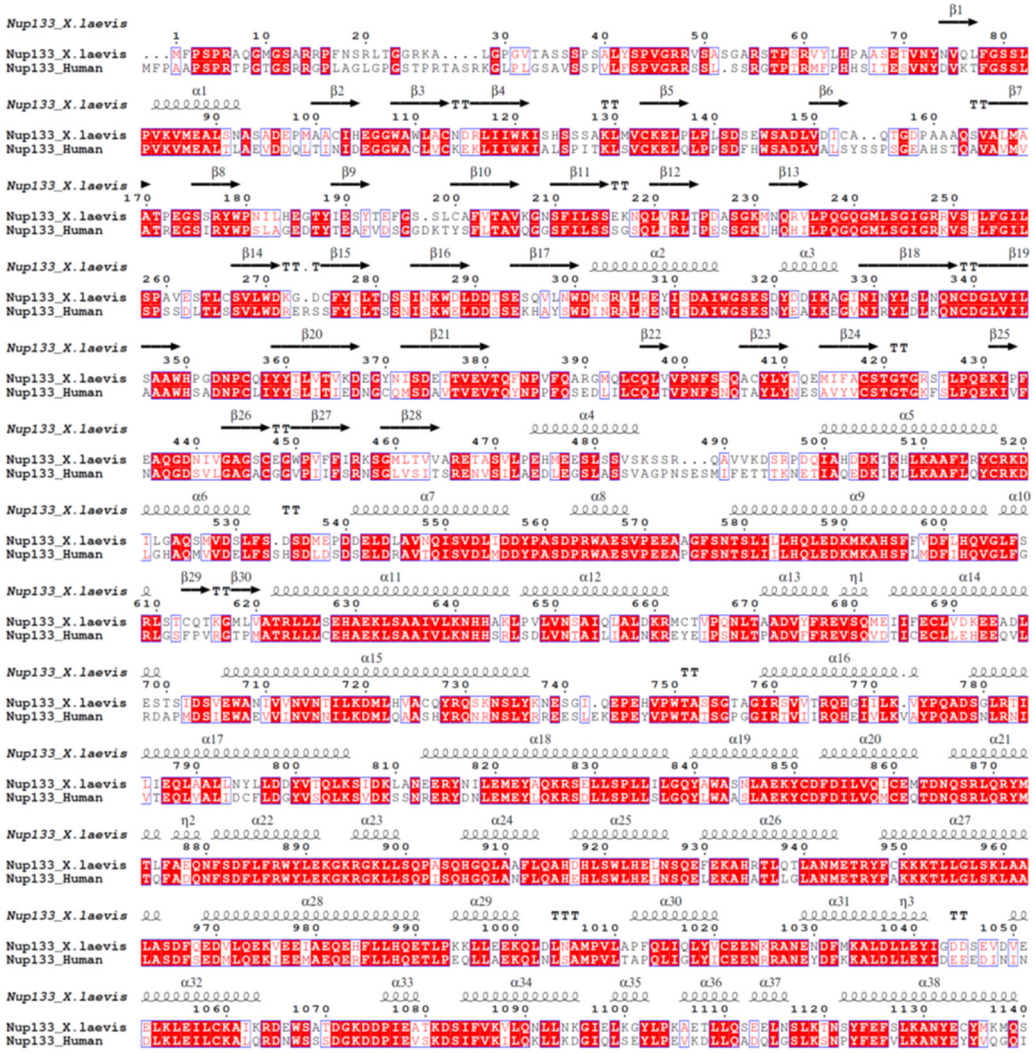

J

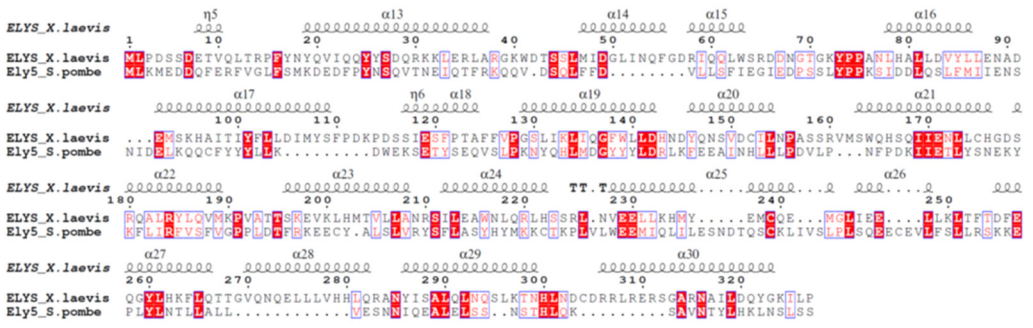

K

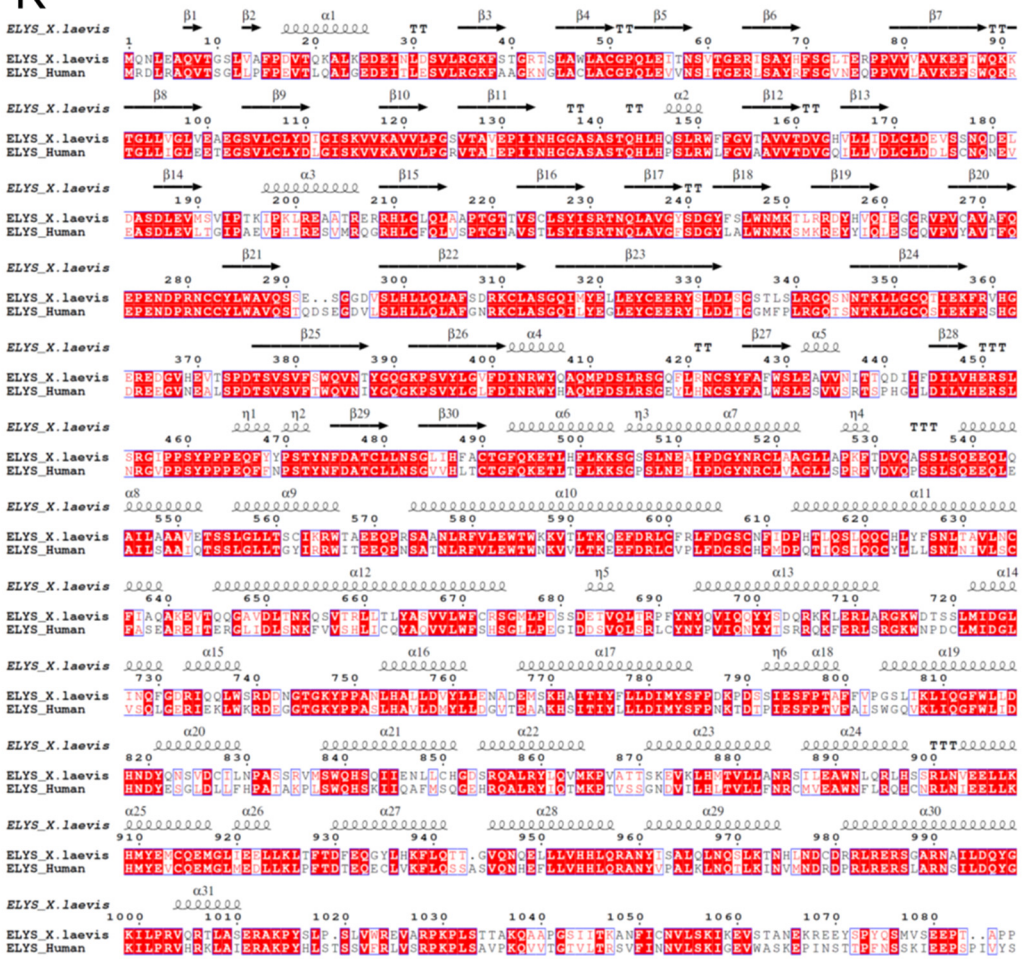
ELYS_X.laevis
ELYS_X.laevis
ELYS_Human
ELYS_X.laevis
ELYS_Human
ELYS_X.laevis
ELYS_Human
ELYS_X.laevis
ELYS_Human
ELYS_X.laevis
ELYS_Human
ELYS_X.laevis
ELYS_Human
ELYS_X.laevis
ELYS_Human
ELYS_X.laevis
ELYS_Human
ELYS_X.laevis
ELYS_Human

L

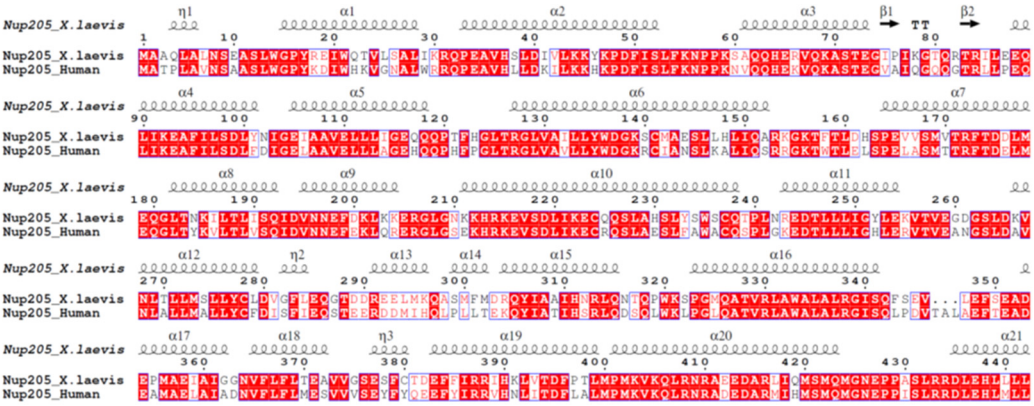
Nup205_X.laevis
Nup205_X.laevis
Nup205_Human
Nup205_X.laevis
Nup205_Human
Nup205_X.laevis
Nup205_Human
Nup205_X.laevis
Nup205_Human
Nup205_X.laevis
Nup205_Human
Nup205_X.laevis
Nup205_Human

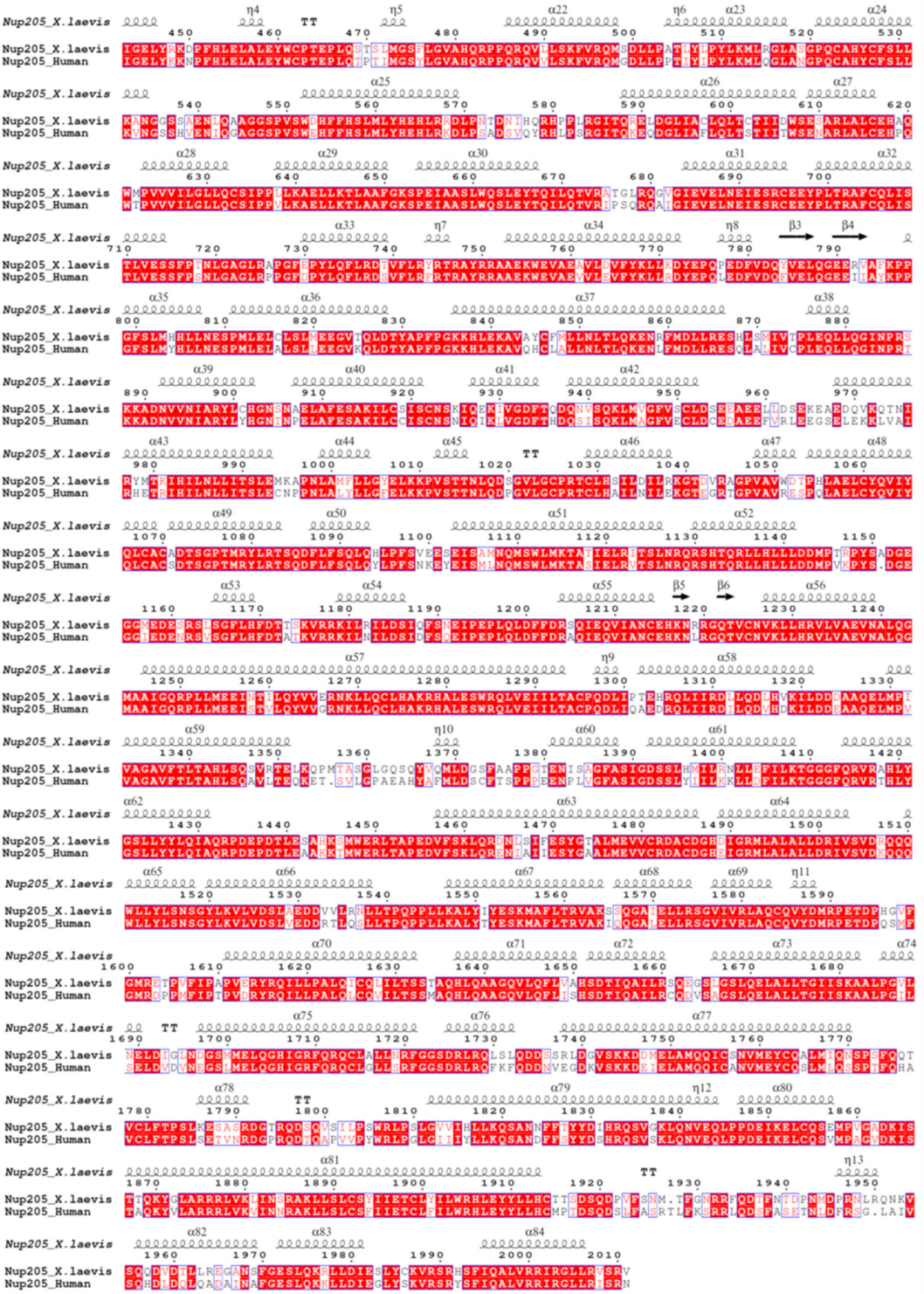
Nup205_X.laevis
Nup205_Human


M
Nup93_X.laevis
Nup93_Human
N
Nup214_X.laevis
Nup214_Human
O
Nup62_X.laevis
Nup62_Human

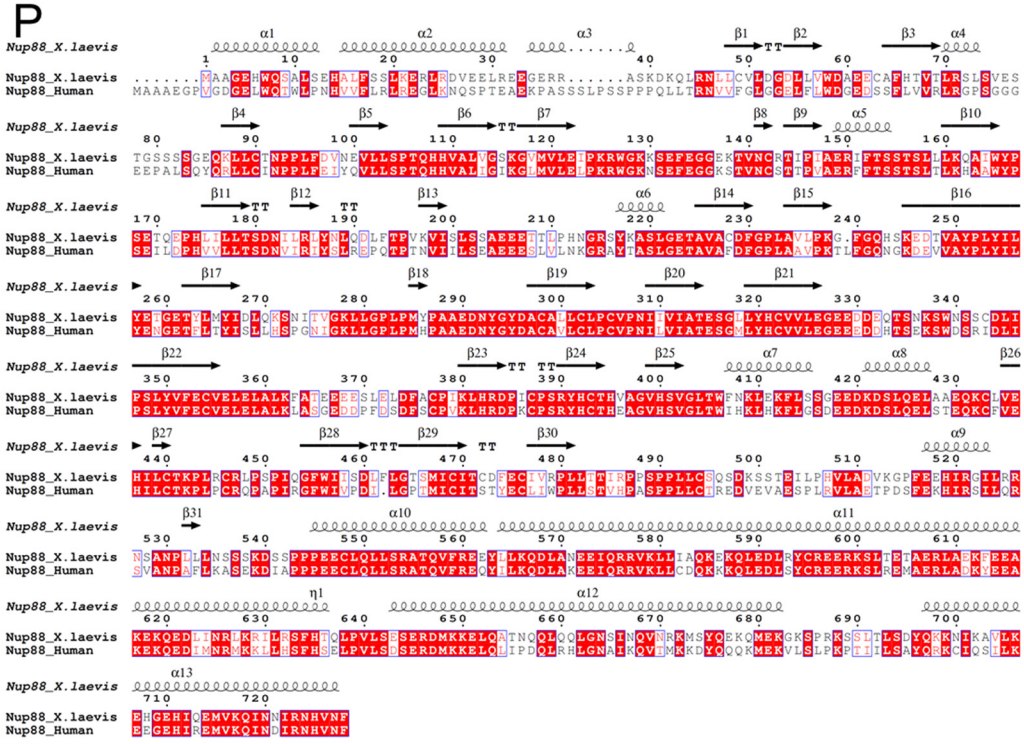
P
Nup88_X.laevis
Nup88_Human
Q
Nup358_X.laevis
Nup358_Human

R

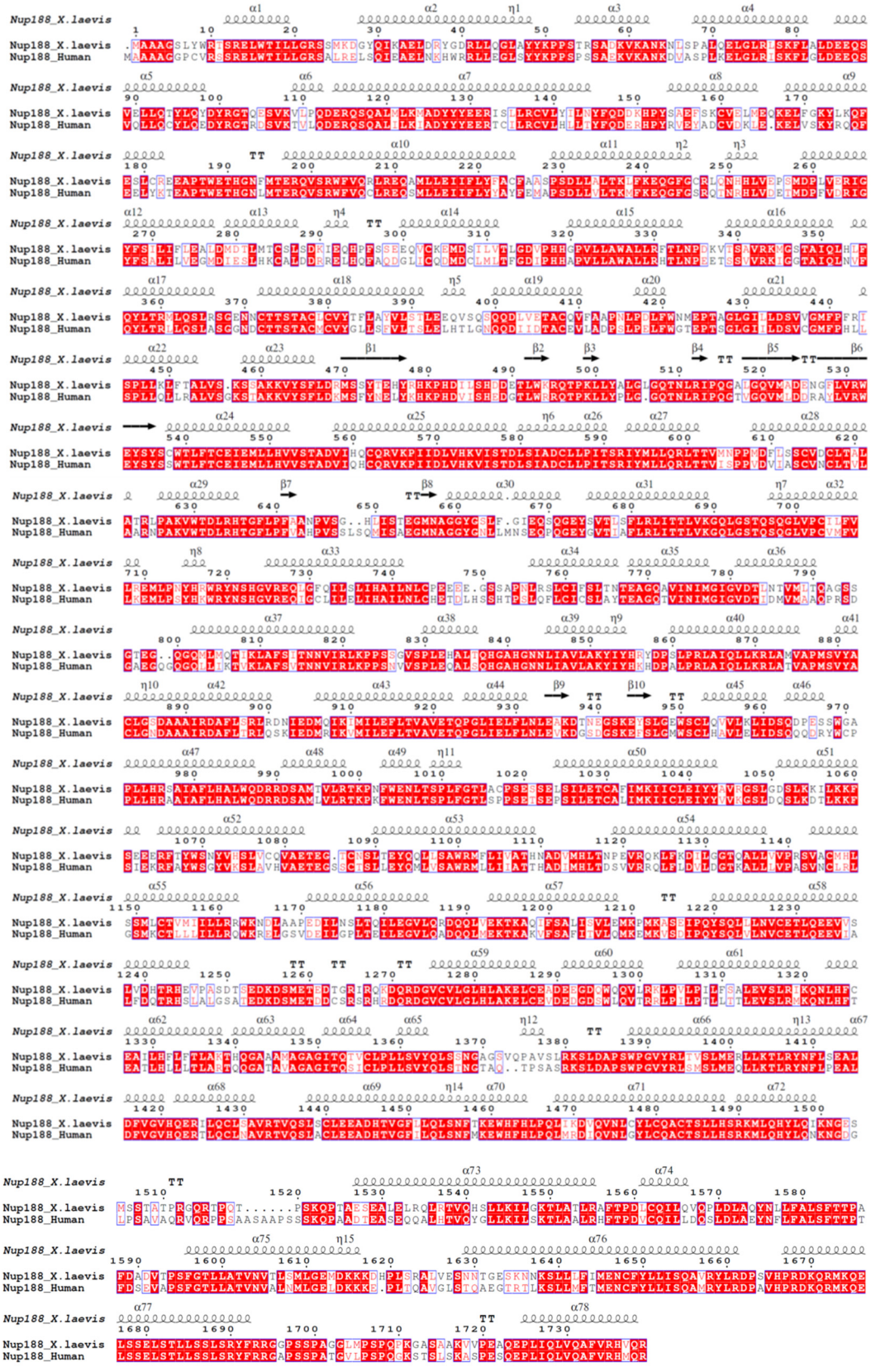

Figure S13. Sequence alignments of Nups in CR and NR from *X. laevis* (or *X. tropicalis*) and human NPCs.

Table S1 Statistics of cryo-SPA data collection and image processing.

Data acquisition			
Microscope	Titan Krios G2		
Voltage (kV)	300		
Detector	Gatan K2		
Energy filter	Gatan GIF Quantum, 20 eV		
Mode	Super resolution		
Pixel size (Å)	2.24		
Stage tilting angle	30°/ 45°/ 60°/ 0°(side-view)		
Exposure per tilt (e/Å²)	60 / 80/ 100/ 100 (or 120)		
Number of images	8745		
Defocus range (μm)	-1 ~ -4		
Software	SerialEM		
Reconstruction in CR			
Software	RELION-3.0/CryoSPARC		
Data set	CR core region	CR subunit region	CR Nup358 region
Final number of particles	354460	354460	678866
Symmetry	C1	C1	C1
Final resolution (Å)	8.0	8.7	8.9
Map pixel size (Å)	2.24	2.24	2.24
Map sharpening B-factor (Å²)	-591	-763	-850
Reconstruction in NR			
Software	RELION-3.0/CryoSPARC		
Data set	NR core region	NR subunit region	NR Nup133 region
Final number of particles	417490	417490	298318
Symmetry	C1	C1	C1
Final resolution (Å)	7.8	8.1	8.6
Map pixel size (Å)	2.24	2.24	2.24
Map sharpening B-factor (Å²)	-433	-541	-612

Supplementary Movies.

Movie S1. Overall structure of outer rings from the *X. laevis* NPC.

Movie S2. Model-map fitting quality of CR Nups from the *X. laevis* NPC.

Movie S4. Model-map fitting quality of NR Nups from the *X. laevis* NPC.

Movie S4. Structural comparison of Nup93 between the refined model and the model predicted by AlphaFold2.

Supplementary Scripts.

Script S1. The modified block-based reconstruction script for symmetry expanding of CR and NR asymmetric units.